PREPARATION AND CHARACTERIZATION OF A TREATED MONTMORILLONITE CLAY AND EPOXY NANOCOMPOSITE

Peter Robert Butzloff, B.S.

Thesis Prepared for the Degree of

MASTER OF SCIENCE

UNIVERSITY OF NORTH TEXAS

December 2000

APPROVED:

Nandika Anne D'Souza, Major Professor
David Crane, Committee Member
Teresa Golden, Committee Member
Rick Reidy, Committee Member
Bob Wallace, Committee Member
Bruce Gnade, Committee Member, and Chair of the Department of Materials Science
C. Neal Tate, Dean of the Robert B. Toulouse School of Graduate Studies

Butzloff, Peter Robert, Preparation and Characterization of a Treated Montmorillonite Clay and Epoxy Nanocomposite. Master of Science, (Materials Science), December 2000, 97pp, 4 tables, 43 illustrations, 43 references.

Montmorillonite reinforced polymers are a new development in the area of nanocomposite materials. Since reinforcement of epoxy is important to the development of high strength adhesives and composite matrices, the introduction of montmorillonite to epoxy is of interest. Compositional effects on epoxy reactivity, on molecular relaxation, and on mechanical properties were investigated. Change in reactivity was determined by Differential Scanning Calorimetry. Tensile properties at room temperature indicated improved modulus and retention of strength of the epoxy matrix but a decreased elongation to failure. Depression of dry nanocomposite glass transition was observed for nanocomposites beyond 5% by weight montmorillonite. Samples that were saturated with water showed lower moduli due to the epoxy matrix. The greatest moisture absorption rate was found at 7%, the least at 3%.

Your strength is in a bubble caught.

By Peter Butzloff

Adobe bricks in Caesars' time
like bathtub fun or strength in rhyme
last for generations come
like scum or gum as stone become.
But some of us who share this earth
Would take a newer loam to berth.

Imagine we can structure clay
to swell with plastic, if it may.
Fear of water runs amok
in micelles to distress this muck
but just like bubbles new shall sway
it tests of time the olden way.

We can build our house of cards
but card or clay could crash to shards.
Ruin comes to those that lilt
Dismay is part of being built.
Examine how the bricks should stack
and tell me how like cards they pack.

So if we think in nanoscale
or build a wall of nanoshale
don't deny a porous thought!
Your strength is in a bubble caught
in volumes cast to tell of tales
that oriented life unveils.

The Romans did it with an arch
but who now speaks of Ides in March?
Nanotubes we now discuss
because today they make a truss
that fits between a layered clay
like filaments of carbon hay.

We set our silicate to ride
on crack where weakness likes to hide.
Lend your bubble for support;
the nanonet can but contort.
The bend of carbon ropes rebound
as bubbles butress all around.

Request the tubes of carbon sticks
to scaffold in our micro-bricks.
Burst the bubbles in the broth
at peril to the bliss of froth.
No foaming blast comes from my mouth
in stronger form from north to south.

Yet in our strength it's voids we share,
and of our Nature we beware.
Networked in a common ground
together might our strength be bound,
so build where bubble dragons fly
and set these bucky bricks nearby.

ACKNOWLEDGEMENTS

To all of my instructors: they imparted important technical wisdom and scientific knowledge. For their dedicated assistance with electron microscopy, David Garrett and Prakaipetch Punchaipetch are gratefully acknowledged.

The friendly support of other students was greatly appreciated.

Bruce St. Romain II deserves acknowledgement for his very patient instruction in the fine art of correctly machining mechanical test specimens.

To Dr. Tie Lan, of Nanocor, Inc. for insightful technical discussions.

To Bell Helicopter Textron, for the use of much test equipment and permission keep very unusual hours to meet schedules.

For time not spent together so that this work might be achieved, I wish to acknowledge the love and support of my wife Marion and the acceptance given by each of our five children.

TABLE OF CONTENTS

Page

LIST OF TABLES

LIST OF ILLUSTRATIONS

LIST OF EQUATIONS

EQUATION Page

CHAPTER 1

INTRODUCTION

1.1 Montmorillonite and polymer nanocomposites

The development of clay platelet reinforced polymers has attracted interest due to improved fire resistance, tensile modulus, moisture and gas barrier properties, as well as improved dimensional tolerance (1). These improvements are achieved through montmorillonite modification due to the remarkable level of particle interpenetration by polymers. Montmorillonite chemically treated by ion exchange permits its combination with polymers on a nanometer scale (2). Each clay platelet may be considered an oxygen-silica polymer that is very stiff. The silicate has sufficient covalently bonded character to make an excellent match to the covalent nature of most carbon based organic compounds.

Layered silicates belong to the family of 2:1 layered silicites (3,4). The crystal structure consists of two silica tetrahedra fused to an edge shared octahedral sheet of either alumina or magnesia (3,5). Each layer is composed of a sheet of aluminum or magnesium octahedra sandwiched between two sheets of SiO_4 tetrahedra, which has a unit cell structure consisting of 20 oxygen atoms and 4 OH groups. These layers are continuous in the a and b directions and are stacked one above the other in the c direction. The crystal structure consists of layers made of two silica tetrahedra fused to an edge

shared octahedral sheet of either alumina or magnesia. Stacking of these layers lead to a regular van der Waals gap between them called the interlayer or gallery. Isomorphic substitution within the layers generates negative charges that are normally counterbalanced by cations residing in the interlayer. Pristine layered silicates usually contain hydrated Na+ or K+ cations. These can be replaced by ion exchange reaction with cationic surfactants, including primary, tertiary and quaternary ammonium to render the normally hydrophilic silicate surfaces organophilic. The basal spacing can be changed depending on the nature of the exchanged cations, the degree of solvation and/or the size of the organic molecule.

The purpose of the pretreatment is to increase the interlayer spacing as well as to provide better polymer compatibility. Swelling of the clay is called intercalation. As the silicate layers move apart, regular spaces between layers can still be maintained. The transport of polymer mass into this space, or gallery, is what determines the rate of intercalation.

Exfoliation is a sufficiently large distortion of already intercalated clay so that individual platelets move very far apart from each other into the matrix polymer. On exfoliation the layers are no longer closely associated with or parallel to each other. The exact distance will vary with the type of polymer used and the surface interaction of the clay with the polymer. This morphology will start to happen at about 60-nanometer platelet spacing for epoxy clay, and is complete at 80-100 nanometers when the layers are irregularly separated as indicated by an absence of Bragg x-ray scattering (18).

Unfortunately, the intercalated state may not be stable in some mixtures. It is possible for some polymers to intercalate treated clay yet not exfoliate it. The polymer

and the clay treatment must be able to overcome the clay platelet attractions to be able to exfoliate. Both intercalation and exfoliation happen on a molecular level.

1.2 Scope of work:

Since the epoxy matrix is a reactive component, the reaction kinetics were determined by diferential scanning calorimetry (DSC). The nanocomposite mechanical properties must be understood in terms of the overall domination of the matrix or the clay reinforcement. Concentration effects on mechanical behavior were determined by dynamic mechanical analysis (DMA) to quantify change in the glass transition temperature. To be effective, the clay additive must be integral with the matrix. This would enable the microstructures to bear significant load. A good dispersion would permit large surface areas of mechanical contact for each platelet with the resin matrix; therefore Dynamic Mechanical Analysis (DMA) data was used to plot the shift factors versus the temperature of deformation for various concentrations of nanoclay. Tensile tests were conducted to provide insight into the concentration dependence of the clay platelets on the strength and ductility of the resin. Samples were also moisture conditioned to saturation to check for structural or concentration effects on the barrier properties, and to check for the effect of moisture on the reduction of strength.

Scanning electron microscopy (SEM) was conducted to determine the clay platelet agglomeration morphology. Transmission electron microscopy was conducted to determine the clay platelet spacing in the agglomerated particles. This trend was confirmed by differential scanning calorimetry (DSC).

CHAPTER 2

LITERATURE SURVEY

To insure adequate interaction between clay particles and polymers, ion exchange treatments have been a central issue in the research of polymer-montmorillonite nanocomposites. The rate of polymer intercalation of treated clay was initially investigated for reactive epoxy (6-12). A growing body of research is now also focusing on intercalation of reactive urethane (13) and polymer melts (14-16). Determination of epoxy intercalation with and without the presence of hardener has brought the most understanding of the chemical and the physical mechanisms involved in intercalation (17-20). Molecular scale reinforcement of polymer has been a desirable way to increase mechanical properties (21-24). Void inclusion due to the high surface area of the clay is however expected to degrade mechanical properties (23, 25-30). Other interactions such polymer wetting (31), T_g (2), particle orientation (18), constrained environments (32), and plastization (33) may also effect nanocomposites.

Primary amine functionalized alkylammonium cations were first shown to improve epoxy wetting of montmorillonite clay sufficiently to induce intercalation (6). This surfactant treatment works by lowering the surface energy of the silicate layers. The ion-exchanged surfactant is anchored to the solid clay surface. An early comparison was made of primary alkylammonium ions that have different acidic strength on the ability to intercalate montmorillonite (7). This study found it was not the lability of the hydrogen,

but rather the structure or bulk of this ion that seemed to control the accessibility of epoxy into the gallery space. More cations might be thought to improve the organic wetting of clay. A limit to the number of ion exchanged molecules is finally reached that depends on the radius of the exchanged cation and not on the charge density of the clay (8). Finally, too much charge density on the clay was found to interfere with monomer or polymer to work into the gallery area between the clay plates for intercalation because in this case, electrostatic attraction makes clay platelet separation more difficult (8).

The cation length, not the number of cations, defines the distance that separates the platelets to achieve intercalation. This defines the secondary role of the alkylammonium cation to act as a pillar. Regular formula addition of carbon atoms increases the length of the onium ion. This fact was used to demonstrate regular alterations in the extent of epoxy swelling (12). The effect of chain length on clay swelling appears to hold true for other systems such as polyurethane (13). Finally, it was found that the molecular weight of the polymer affects the rate of the intercalation but not the final layer spacing (14).

Theoretical analysis by Gianellis (15) did much to help elucidate the nature of the competitive forces at work in terms of the dispersion phase stability. The competitive forces on the intercalated polymer were understood as follows. A change of the clay volume fraction alters the apparent interaction parameter. This results in a drawing out of the polymer from the gallery interlayer. At some concentrations polymer will then prefer to participate in the more favored state outside the gallery. This immiscibility turns the treated clay into ordinary filler since it can not act as a true lateral nanoscale reinforcement. By changing the interaction parameter particle layering by charge

orientation can then take place so that structures that bond to organic components are less dominant.

A new strategy was required to keep monomer or polymer between the silicate layers at all concentrations. Messersmith and Giannelis found the first practical solution for epoxies (17). In contrast to all previous work with intercalation of non-reactive polymers, they bonded epoxy-intercalated clay with reactive hardener to improve the strength of the clay-polymer interface. It was not clear from that study if this was a physical or a chemical bond, but arguments for both cases were presented. The significant result was that the reaction during cure could stabilize intercalation of the clay at all concentrations. This approach had the additional desirable effect of producing extensive amounts of the exfoliated state (18).

Contrary to the initial suggestion of Messersmith and Giannelis (17), epoxy polymerization does not proceed by reaction with with acidic primary alkylammonium ion-exchanged cations in the treated clay as first suggested in that work. It was later clarified (19) that the epoxy reaction at the surface of treated clay results in a self-polymerization hydrolysis reaction of the epoxy due to opening of the strained epoxide ring. This clarification was required to permit the exclusion of the chemical contribution of the amine present in the primary alkylammonium cation as a competitive reaction to the amine hardener that is introduced for epoxy-amine polymerization. A similar clarification has apparently not been made for the secondary amine alkylammonium cation reaction with epoxy monomer in montmorillonite silicates.

The reactive group-alkylammonium ion polymerization conjecture of Messersmith and Giannelis (17) remained important because later work with tertiary

alkylammonium ion-exchanged cations (13) found that these species, unlike their primary alkylammonium cation counterparts, have indeed crosslinked into reactive polyurethane systems.

It was recently shown by thermogravimetric analysis that a secondary alkylammonium cation used to treat a layered magadiite silicic acid incorporates into an epoxy chemical network (20) to cause unprecedented exfoliation of that system. Several significant observations were made. Similar to the case of treated montmorillonite (8), a treated magadiite will not form a covalent chemical bond with epoxy when a primary alkylammonium cation is used (20). Care must be taken that less than 10% of the secondary alkylammonium cation is used to permit network formation with the epoxy and the hardener. Mechanical properties for this related layered silicic acid nanocomposite were reported to be inferior to the 2:1 smectite silicate epoxy nanocomposites due to the reduced stiffness of the magadiite silicic acid sheets.

Improvement to the mechanical properties of polymers is possible when stress transfers from the matrix to the reinforcement. One way this can happen is for two interpenetrating molecular phases to have a network structure where one of these is sufficiently unconstrained to permit plastic deformation (21). In clay nanocomposites, rigid particle toughening of epoxy may be possible due to the impedance of crack growth (22). A discrepancy exists between experimental modulus (11) and the theoretical modulus improvement based on an effective aspect ratio (height / area) of clay platelets in polymer nanocomposites (23).

An individual clay platelet can be as thin as 1 nanometer and may be less than a micron long in any of the other two dimensions. This can translate to a great deal of mobility for the particle as a chemical unit when it is sufficiently dispersed into a liquid. Charge on suspended clay particles in the natural state is understood to cause their association into larger groups called flocs when they are suspended in water (4). This usually results in sedimentation of the suspension over a long enough period of time. A recent scanning electron microscopy (SEM) study of treated clays in reactive polyester found the only dispersion morphology was a flat and platey one (24).

Transmission of gases and moisture vapor through polymers by the incorporation of clay silica platelets has been shown to decrease their permeability (25). Void inclusions can significantly reduce the reinforcement that is theoretically possible (23) due to a reduction of the polymer clay interface, especially if the voids are not isolated (26). For these reasons conditions are usually identified that minimize gas voids but do not cause serious interference to the preparation. In cured epoxy without reinforcement, the kinetic transport of moisture at the initial stages of transport appears to be related to nanovoids that may exist in epoxy resins (27). This is seems not to apply to later stages of moisture uptake, where the amount of polar interaction sites (28), polar ion impurities (29), and volume expansion stress at epoxy reinforcement interfaces (30) dominate the moisture uptake in epoxy.

Polymer wetting of clay platelets is important to the mechanical properties of composites formed from them. The first theoretical analysis based on microstructure for wetting (31) on the viscoelastic properties of rough particle surfaces was provided by

T.S. Chow in 1998. This theory relies on an analysis of surface tension by changes in contact angle that are due to the roughness of the particles.

Particle wetting can only partly explain why the mechanical properties of epoxy nanocomposites have shown mixed results to date. For an epoxy resin cured with m-phenylenediamine marginal improvement in mechanical properties was reported (8). The limited improvement in this study was tied to the high T_g of the epoxy matrix. Subsequent work targeted a low T_g epoxy that was hardened with Jeffamine D2000 polyether amine (Huntsman Chemical Corp) to obtain a sub-ambient T_g (2). For each of these studies clay was added to the mixture of resin and hardener. Tensile modulus was increased from 2.5 MPa for the base epoxy resin to 7.5 MPa for 5% clay. The increase in strength for low T_g epoxy was partly attributed to a natural increase of plasticity due to the presence of nanoclay. The increase in strength at large strain was attributed to nanoclay platelets that could orient above the T_g in the direction of the strain field to provide reinforcement in the direction of extensional deformation (18).

Harrowell's review of the effect of constrained polymer environments (32) suggests that polymer films between strongly adsorbing mica layers can appear temporarily rigid well above T_g, depending on the angle between mica sheets. This affects the local microstrain required to overcome or "soften" the rigid film state. This state appears in polymer film thickness below 5 molecular diameters, where the film mechanically resembles a gel in terms of low shear modulus and yield stress.

Manne and Warr have reviewed the role of surfactants on ion exchanged silicate surfaces (33). Some studies in that review suggest that the ion exchanged surfactant on the clay might undergo liquid crystalline transitions at their surfaces depending on ion

exchange density and the nature and length of the pendant surfactant. This helps to understand why plastization effects may be observed under some conditions for treated clay nanocomposites.

CHAPTER 3

EXPERIMENTAL

3.1 Materials

The epoxy resin used was a Bis-phenol A diglycidylether Epon 828 from Shell Chemical company. The hardener was an amine curative hardener, Jeffamine D-230 provided by Huntsman Chemical Corporation. The chemical name in IUPAC format is Poly (oxy (methyl-1, 2-ethanediyl)), alpha- (2-methylethyl) omega- (2-aminomethylethoxy)-amine. The clay provided by Nanocor is octadecylammonium salt of Montmorillonite, a derivitized form of bentonite clay designated I30.E.

Pure aluminum silicate is $4SiO_2 \bullet Al_2O_3 \bullet H_20$. The form of aluminum silicate known as montmorillonite has Mg^{+2} impurity substituted at some of the sites of Al^{+3} with a general form reported by (9) as:

$$(R+) \bullet (-)[Mg_x\, Al_{4-x}](Si_8)\, O_{20}\, (OH)_4]$$

where R is an intercalated cation of valence n that may substitutes for Ca or Na in the native clay in quantities of x/n. This montmorillonite will also be referred to as nanoclay. Chemical analysis of the nanoclay ash used in this study revealed 0.0031% Magnesium and 0.1787% by weight of Aluminum:

$$[CH_3\,(CH_2)\,17NH_3(+) \bullet (-)[Mg_{\,0.54}\,Al_{\,3.38}](Si_{\,7.64}\,Al_{\,0.36})\, O_{20}\, (OH)_{\,4}]$$

3.2 Sample preparation

There are several approaches to prepare nanocomposites for reactive polymer systems with two components. Nanoclay may be mixed into either the hardener alone, into the resin monomer alone, or into a reactive mixture of resin and hardener. In all cases mix completion is estimated by placing a drop of the mixture between optical microscope slides to verify the absence of undispersed clumps in the mixture. Each approach is limited to a different extent.

Ultrasonic treatment has been recognized as an aid to speed diffusion of polymer into nanoclay (17). What has not been sufficiently appreciated is the danger of forming local hot spots from reaction at poorly dispersed areas of nanoclay that are exposed to ultrasound. This effect is worse at high concentrations of nanoclay and at elevated temperatures. This disadvantage is overcome by limiting the use of ultrasound to low temperatures where reactivity is not an issue. In all cases vacuum degas is widely recommended (34) to remove gas inclusions from the mixture prior to polymerization.

It is not desirable to mix the nanoclay into a two-part mixture of both resin and hardener. The upper temperature and time limit for a typical process reaction is altered. For the time required to ensure a good dispersion the material polymerizes before introduction to a mold due to a reduction in pot life. This effect was most pronounced at concentrations greater than 5% by weight of montmorillonite in a three-part mixture. Test for enhanced reactivity in the presence of the clay was therefore necessary. This effect may be desirable to reduce reaction temperatures if it is identified and taken into account.

To avoid sedimentation of the clay, it was found necessary to add it to the epoxy resin rather than the hardener. Clay sediment forms from the hardener when stirring stops, making it difficult to redisperse. Dispersion of clay into epoxy was therefore used to prepare the premix. To achieve lower epoxy viscosity and improve dispersion, the mixing was performed at 80°C. The temperature must be kept below 85°C or a waxy consistency will form making it unworkable.

That portion of clay in the epoxy monomer prior to the addition of hardener shall be referred to in this work as the "resin pre-mix". The percent by weight of nanoclay would be different for a mixture of resin monomer than for nanoclay in the resin and hardener together. The three-part mix is made by addition of the premix to the hardener. The "three part mix" is defined as the weight percent of montmorillonite in all three parts. Equivalent weight and volume percent calculations are shown in Table I.

Table I

Concentration equivalents

Nanoclay part of premix (clay + resin)		Nanoclay part of 3-part mix (clay + resin + hardener)	
% by wt.	% by vol.	% by wt.	% by vol.
1.4	0.8	1.0	0.9
2.8	1.6	2.0	1.8
3.5	2.0	2.5	2.3
4.3	2.4	3.0	2.7
7.3	4.0	5.0	4.4
9.6	5.7	7.0	6.0
15.4	8.1	10.0	8.3
24.4	12.3	15.0	11.7

Epoxy resin was mixed with silicate nanoclay for 1 hour at 80°C. The premix was then vacuum degassed at 38mm of mercury to the onset of resin boil, then returned to atmospheric pressure and allowed to cool to room temperature. Aliquots of the resin and nanoclay premix were set aside for the DSC test. Jeffamine hardener was then added in stoichiometric proportion to the epoxy in the premix to create the "three part mixture". Epoxy - nanoclay three part mixtures containing 1, 2, 2.5, 3, 5, 7, 10 and 15% by weight nanoclay were prepared. Aliquots from of each of these preparations were cryogenically stored at (-65°C) for later DSC test.

A final degas of the three part mixture was required prior to cure due to gas inclusion when mixing in the hardener. Panels were then cast from each three-part mixture in open top rectangular solid molds prepared with a Teflon release. The cure was for twelve hours at 60 ^{o}C. The panels were then post-cured at 105°C for 12 hours to ensure cure completion.

3.3 Machining

Rectangular thin section slices cut from each cast resin panel with a water-cooled carbide saw. The direction of cut was parallel to the cast mold bottom surface. Tensile dogbone specimens were prepared from these by mounting several specimens between two metal preforms, then using a router the excess resin was removed near the middle sections to obtain the dogbone dimensions.

Cut specimens were dried at 105°C overnight to remove trace amounts of water and perform the stress relaxation called out in ASTM D5229 prior to test of moisture

conditioned polymeric specimens. All of the test specimens were at room temperature prior to mechanical test.

3.4 Humidity Uptake and conditioning

A Thermotron model F-30 Environmental Chamber equipped with a Honeywell Trueline recorder/controller was used to generate the humidity conditions for the study of the effects of moisture absorption on the nanocomposite. The system was operated at 355°K (82°C) and 95% relative humidity. Measurements were taken in accordance with ASTM D5229 to determine moisture absorption and the equilibrium condition of the polymer matrix composite material. The important criteria called out in the method indicates that specimens used for this test be all the same size, thickness, and shape for a valid comparison to be made.

"Wet conditioned specimens" shall be used to define and refer to the tensile specimens that were subjected to humidity. Wet conditioned specimens were removed from the environmental chamber and permitted 30 minutes to come to constant weight prior to weight determination. All time spent outside the chamber at room temperature for weight determination was subtracted and not counted toward the accumulated duration at moisture exposure. These test panels were set into custom made racks designed to maximize exposed surface area, permit airflow between specimens, and maintain a canted surface to avoid any possible pool of liquid droplets on the flats of the test specimen.

The purpose of the moisture study was to obtain tensile specimens at the maximum or worst case moisture absorption. By conducting the moisture conditioning well above the T_g the matrix effects were standardized for all samples. The elevated

conditioning temperature was estimated to be capable of achieving the saturated condition in a reasonable time.

The wet conditioned specimens were a subset of the tensile dogbone specimens prepared for both the purpose of determining the moisture absorption rate to saturation as well as the mechanical test results for the worst case water absorption scenario. Engineers often use this approach for determination of the worst case property reduction for the purpose of part design.

3.5 Differential Scanning Calorimetry (DSC)

DSC was conducted on a Rheometrics High Temperature Model PL-DSC. For this test, a 5-mg sample was sealed into a crimped aluminum pan and heated in conjunction with an empty aluminum pan of equivalent weight. As the heat was supplied to each pan at a constant rate, a matched pair of resistances known as a Wheatstone Bridge electrically detected the differential amount of energy required to change the temperature in both pans simultaneously. Deviation of thermal balance that appears in one of the two pans is caused by a chemical reaction or a phase change in the sample pan that is then amplified to provide a signal of the thermal difference. Indium and tin calorimetric melting point standards were used to calibrate the thermal response due to heat flow as well as the temperature prior to analysis.

The resin premix was tested at a constant heat rate of 5°C/minute from 25 to 300°C to determine the concentration effect of the montmorillonite clay on the opening of the epoxide ring without polymerization of the epoxy.

Reaction kinetics were determined for unreacted three part mixtures of epoxy, hardener, and nanoclay tested at constant heat rates of 2, 5, and 10°C/minute from 25°C

to 290°C. These cured samples were cooled to 25°C with liquid N_2 following testing. They were then equilibrated for 15 minutes at room temperature and scanned a second time at a heat rate of 10°C/minute over the same temperature range to determine T_g and confirm cure completion. The T_g was determined by the midpoint method.

3.6 Dynamic Mechanical Analysis (DMA)

DMA was conducted using a Rheometrics Dynamic Spectrometer model RDS-IIe, with a cryogenic oven. Frequency temperature sweeps were performed between 0.1 - 100 radians / second from -150 to 130°C in 5°C steps. 5 data points per decade of frequency were recorded. Holding at isothermal temperature for 2 minutes prior to data collection ensured a constant temperature.

DMA measures the material response at an end of a fixed sample farthest removed from the location of an applied displacement. Both stress and strain controlled DMA instruments are available. The above DMA equipment is strain controlled, so it applies a known displacement that is compared to the observed sample response.

Perfectly elastic samples would respond instantly to the application of displacement with complete transfer of energy from the displacement to the transducer. The transducer is an electromechanical device to convert positions and force measured from the sample into electrical measurements. When calibrated with known forces and positions, these electrical measurements are converted to signals of stress and strain, respectively. Knowledge of the sample geometry is required to scale the sample stress and strain response, where the sample cross section and sample lengths between the applied and measured deformations are variables that depend on the sample.

For ease of analysis, a simple sinusoidal variation of the deformation is applied to the sample. With stress, strain, the quantitative measure of sample stiffness defined as the material property of modulus may be determined. In the ideal case of a perfectly elastic sample a strain angle difference of 0 radians is observed and no reduction in force is observed, so the applied and measured deformations would overlay perfectly.

The time dependent stress response for a given deformation is known as viscosity. When the sample response lags the applied deformation, the time difference in the applied and the measured sine waves can be quantified by the phase angle difference between them. The viscous sample response to deformation is also somewhat reduced in magnitude. To illustrate this, a strain angle of 0.2 radians phase difference between the applied strain and measured strain is shown in **Figure 1** by the constant x-axis offset of the two sinusoidal curves. In this case a reduction in the height of the sample response illustrates 30% of the applied deformation was not recovered after passing through the sample. A perfectly plastic material would absorb all of the energy of deformation without a detectable force or displacement measured at the transducer.

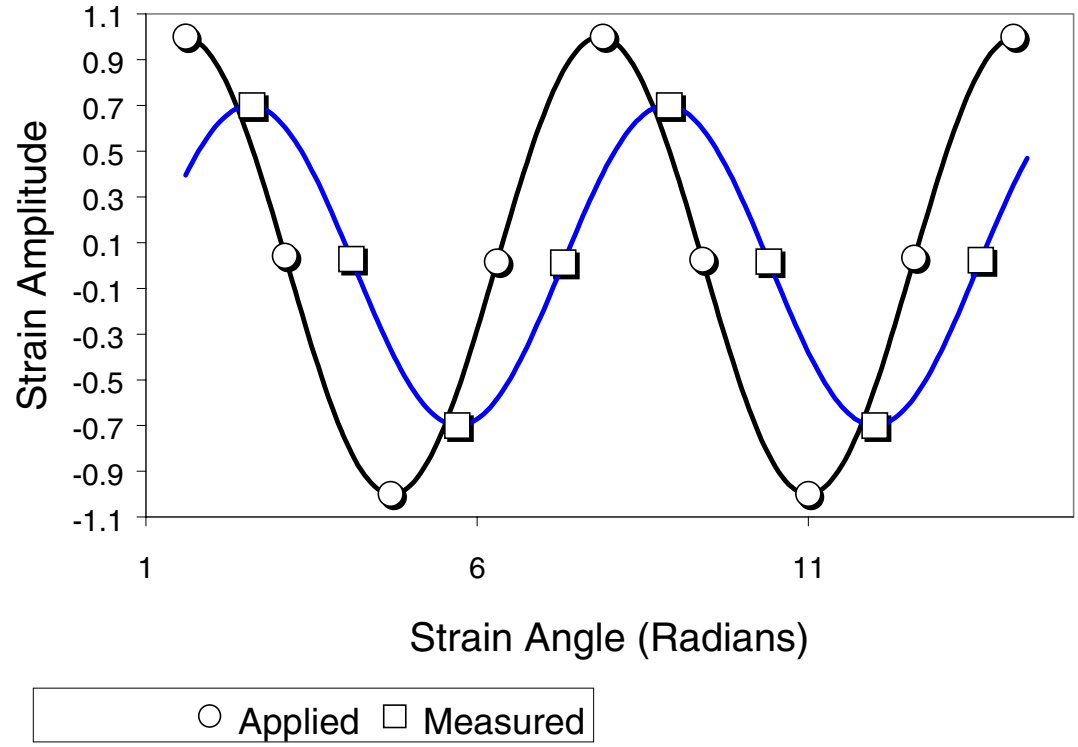

Figure 1 **Viscoelastic response to sinusoidal deformation**

The complex modulus may be thought of as measure that combines both the contribution of the real elastic response (stored) and as well as the imaginary (lost) component as expressed for shear deformation in **Equation 1**:

Equation 1 $$G^* = \sqrt{\overline{(G')^2} + (G'')^2}$$

Where:

G'' = Viscous (or loss) modulus

G' = Elastic (or storage) modulus

The amount of energy lost on shear deformation is that component of the material response that is out of phase with the applied sinusoidal deformation:

Equation 2 $$G'' = \left(\frac{\tau}{\gamma} \right) Sin(\delta)$$

Where:

τ = Shear stress

γ = Shear strain

δ = phase angle difference between applied and measured strain

The component of the material response that is in phase with the applied deformation is given by:

Equation 3 $$G' = \left(\frac{\tau}{\gamma} \right) Cos(\delta)$$

In dynamic mechanical analysis, the glass transition can be quantified by maximal energy loss (G") due to deformation of the material. An impurity such as a small molecule can interpose between polymer molecules to prevent large-scale cooperative motion of the polymer and sterically (physically) reduce the effective free volume into which parts of the polymer molecule may move. This can change the observed T_g by alteration of the free volume to effect the material performance.

The mechanism of T_g, or alpha relaxation, is the onset of large-scale rotational lability of the polymer backbone bonds over the entire molecule. This accounts for largest of the stiff to rubbery change in the elastic material response. The beta relaxation is a transition region associated with group rotation pendant from the polymer molecule. The mechanism of all other relaxations are short-range rotational motion of functional

groups or side chains that depend from the polymer backbone. T_g is not a change of state, such as a melt from solid to liquid, but rather a cooperative molecular change.

When stress is applied to a polymer, stress throughout the material as a distribution of forces that may not immediately be in equilibrium. Two types of relaxation are possible. At low temperatures (below T_g) valence bonds stretch elastically a short distance and then rapidly rebound. One example is the amount of entanglements of side chains to which adjacent molecules may be prone.

In the second type of relaxation at temperatures near and above the T_g the molecular arrangement of bonds are undergoing reconfiguration. This effect is the onset of the cooperative motion of the molecule backbones (the longest continuous chains of bonded atoms in one molecule) due to T_g. The primary source of viscoelasticity in a polymer at or above T_g may therefore be thought of a diffusion of mechanical energy from one molecule backbone to the next.

3.7 Time-Temperature Superposition

Time-Temperature Superposition (TTS) or the shift of modulus in the logarithmic frequency (or time) axis, permits a correspondence of several orders of magnitude change in mechanical response to deformation over a wide range of thermal conditions and time to relaxation. This correspondence is only valid when the thermal history and the mechanical history are each path independent. The state of path independence is called a simple thermorheological state. Possible causes for complex thermorhological states that show a path dependent response are alteration of physical or chemical structure.

A single superposition is illustrated by the frequency sweep data for unfilled cured epoxy with 0% clay shown in **Figure 2**. Here each curve segment represents

modulus found for the same set of frequencies but at different isothermal temperatures. The modulus values measured for 51.8C are intentially plotted twice to indicate a shift to higher frequencies. A constant x-axis term of $\log(a_T)$ was used to permit a best fit overlay of adjacent modulus curve segments. Evaluation of many such a_T shifts to create a single superposed curve are shown later for DMA experimental results.

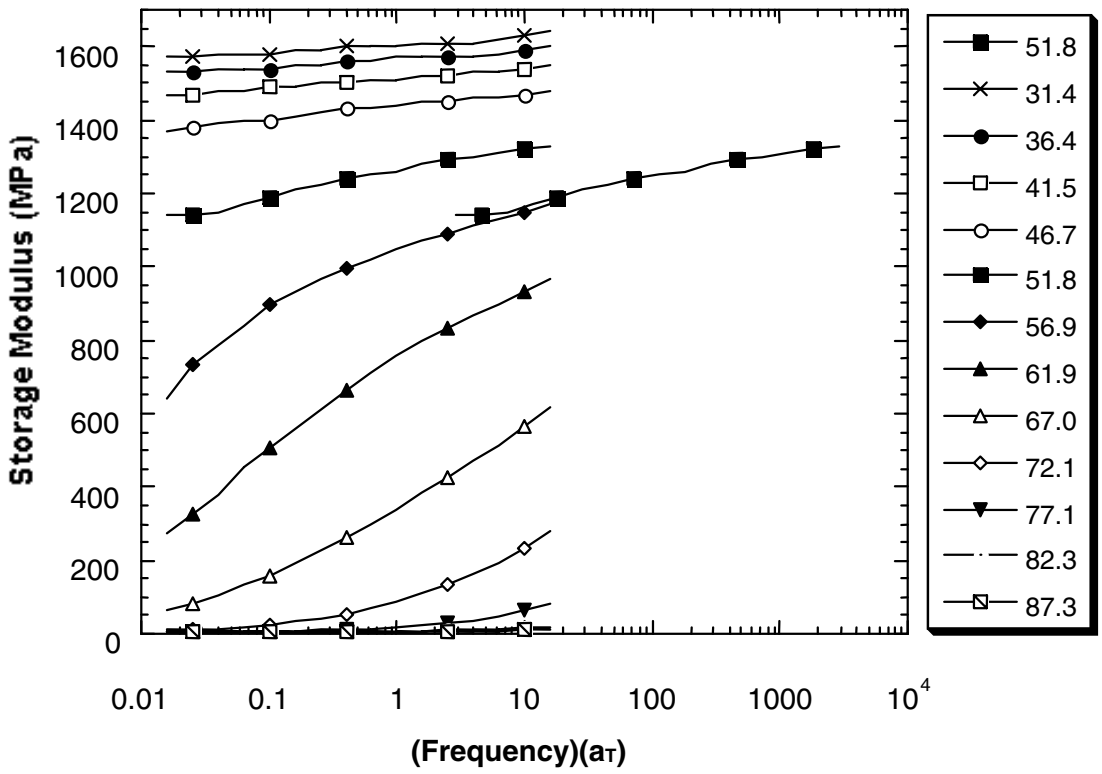

Figure 2 **Use of the shift factor to create a master curve**

When each of the shift factors $\log(a_T)$ is plotted against the measurement temperature over which the shifted data was collected, two trends are observed. The log shift factors are directly related to temperature below T_g, and they are nonlinear with

temperature above T_g. Analysis of the shift factor behavior in both of these of these regions requires an understanding of the mobility of polymer free volume above T_g. The energy of flow activation below the T_g represents a condition of fixed free volume. An analytical summary follows.

For thermorheologically simple materials, at temperatures less than the T_g the shift factor temperature curve follows an Arrhenius relationship as indicated by:

Equation 4

$$Log(a_T) = \frac{H}{R}\left(\frac{1}{T} - \frac{1}{T_{ref}} \right)$$

Where:

a_T = graphical temperature shift factor for superposition

H = activation energy of flow, in KJ/mole

T_{ref} = Temperature of reference, usually taken at T_g.

The interpretation of the activation energy of flow (35) is related to the steepness of the energy barrier that is required to change the quasi-equilibrium state of the system from one configuration to another. If a body were perfectly elastic, the stored potential energy is immediately and completely released when the stress is released. The result is the immediate and complete return of the system to its equilibrium position prior to the stress application. Thus elasticity modulus, shear modulus, bulk modulus and hardness are all functions of the steepness of the energy wells.

At and above T_g, the mathematical expression of the shift factor is given by **Equation 5**, which describes the shift factor in a non-linear manner.

Equation 5

$$Log(a_T) = \frac{C_1(T - T_{ref})}{C_2 + T - T_{ref}}$$

Where:

C_1 = Free volume that is temperature independent.

C_2 = Free volume that changes according to the temperature.

T = Temperature

T_{ref} = Reference temperature used for shift.

According to W-L-F, the constants C_1 and C_2 are dependent on the choice of the reference temperature for shifting. If the reference temperature is the glass transition temperature of a single component system, then $C_1 = 17.44$ and $C_2 = 51.66$. However, since the development of the W-L-F relation numerous researchers have pointed out the lack of universality of these constants. The constants C_1 and C_2 can vary if the reference temperature for shift is not the glass transition temperature. The analytical expression for the free volume clarifies the meaning of C_1 and C_2 as follows:

Equation 6

$$f = f_0 + \alpha_f (T - T_0)$$

Where:

f = the fractional amount of free volume in a given volume

f_0 = the fractional amount of free volume at the reference temperature

α_f = volumetric expansion of free volume with temperature in a given volume of polymer

Ferry has indicated (36) that α_f is very close to volumetric expansion when C_1 and C_2 are defined as follows:

Equation 7 $C_1 = 1/2.303 f_0$

Equation 8 $C_2 = f_0 / \alpha_f$

The W-L-F constants can also change if an impurity such as a small molecule is present to physically interpose itself to hinder cooperative motion of polymer molecules. This hindrance results in a steric reduction of the effective free volume into which the polymer molecule may be able to move or rotate.

These constants measure molecular free volume in two different and distinct ways. C_1 is inversely proportional to the fraction of void, or free volume in the space occupied by a polymer molecule independently of temperature. This temperature-independent term can be further broken down. Another constant that is part of C_1 directly relates the size of the hole available for a small region of the polymer backbone to fit. This effect is usually the same for most polymers, however even the affect of this other constant on C_1 for the same polymer in this study would be transparent. One would not expect C_1 to be affected by any thermal change in the region where W-L-F is valid. C_2 is directly proportional to that fraction of the free volume that must operate on a difference of two temperatures, one being a fixed reference temperature, and the other being the temperature of interest. For the convenience of universal comparison, the fixed reference temperature is chosen to be the characteristic T_g temperature. In summary, the physical meaning of free volume is an unoccupied volume or "free" space into which part of a polymer molecule may rotate or move. C_1 is that part of the unoccupied space that is temperature independent and C_2 indicates what part of this space must depend on temperature.

3.8 X-ray Diffraction

X-ray diffraction was conducted with a Siemans D-500 diffractometer using CuK_α radiation (λ = 1.54056 Å). The tube source was operated at 40 kV and 30 mA. Scans were run between 2° and 35° 2θ at a step size of 0.05° and a 1-second dwell time.

X-ray diffraction analysis is important to the study of nanocomposites because it is presently the only way used to determine how far apart the layers of the clay have been driven in the bulk to quantify the amount of intercalation. The x-ray diffraction peak due to the 001 silicate crystal orientation moves to lower 2θ angles as intercalation increases. In some cases this peak may vanish below the ability of wide-angle x-ray diffraction to resolve, however this is not a problem for small angle x-ray diffraction equipment. Reduction in the intensity of the 001 x-ray diffraction peak where clay concentration remains constant indicates some stacks of silicate platelets have exfoliated and are too disordered to capture the diffraction of the x-rays. Where a good signal is present X-ray diffraction results can attest that platelet separation was successful (37). This is done by comparison of the x-ray diffraction response to partly intercalated clay that is commercially available, and perhaps also to the clay starting material prior to the ion exchange treatment to verify the x-ray diffraction trend.

3.9 Tensile properties

Tensile tests were conducted on an MTS universal test machine at a 5mm per minute constant test rate of crosshead displacement. The test method and sample preparation was in accordance with ASTM D638. The tensile dogbone test coupons were 12.7 mm wide x 3.0 mm thick, cut in parallel with the bottom surface of the cast mold. The tabs on the specimens were 19 mm wide. The gauge length of the specimen was 50 mm. The

narrow part of the specimen was 60 mm long. The overall length of the specimen was 200 mm. Each tab end was wrapped in 1 layer of 300-grit sandpaper to help distribute load from the pointed surfaces of the grip over the specimen tab. Reference were marks placed on the specimen tabs even with the edge of the sandpaper to determine if the sandpaper moved during the test.

3.10 Electron Microscopy:

Transmission Electron Microscope (TEM) model JEM 100CX7 was used to examine microtomed slivers cut with a diamond knife. TEM and the complementary x-ray diffraction analysis were used to determine intercalation and exfoliation as has traditionally been the case. Scanning Electron Microscope model JSM T300 operated at 15 kV accelerating voltage was used to study the fracture surface of tensile dogbone specimens. The fracture surface was cut away from the bulk of the mechanical test specimen with a band saw and mounted to a conductive aluminum stage. Gold vapor deposition onto the fracture surface permitted observation of the microstructure.

In analysis of morphology by Scanning Electron Microscopy (SEM), large structures and particle distributions in the sample are observed, but the small scale order that may give rise to them can not be discerned without the use of TEM or another high magnification method.

CHAPTER 4

COMPOSITION EFFECTS ON REACTION KINETICS

The addition of glass fibers to epoxy has shown a significant effect on the reaction rate is possible due to the nature of the coating on the fibers that make them compatible with the resin matrix (38). Therefore the kinetics of the epoxy cure was investigated to determine the effect that different amounts of treated montmorillonite clay might have on the reaction.

Analysis of the three-part system is simplified when it is possible to observe effects on just two components. Reaction between just the clay and the epoxy was used to clarify the chemical effect of the clay environment prior to the addition of the hardener.

The oxyrane ring is the active functional group in epoxy. This ring becomes unstable and hydrolyses at elevated temperatures. Epoxy ring-opening reaction in resin-clay premix may be effected by different concentrations of clay due to the kind of nanoclay dispersion (19). This study gave evidence that epoxy and nanoclay peaks may split due to a difference in the concentration of reactive acidic onium protons inside the nanoclay gallery compared with the chemical environment outside the gallery. The appearance of two distinctly resolved ring opening peaks were the experimental evidence of the second mechanism.

Typical 2°C/minute DSC test result for the nanoclay and resin monomer premix shown in **Figure 2** confirm that concentration does shift the ring opening reaction to a

lower temperature. No evidence of peak splitting appeared at the high resolution possible for this low heat rate. The single peak observed for 2, 5, and 10°C/minute indicates acid protons from inside or outside the nanoclay galleries behaved no differently in an attack of the epoxide ring. It was therefore concluded that the gallery environment alone could not explain other effects that may be observed by addition of hardener to react with the epoxy in the presence of the clay.

One important difference in the preparation was the 80°C and 1 hour shear used here, as compared with the 75°C for 1-hour shear where peak doublets were reported. A better dispersion at the elevated temperature may explain the desirable single peak results.

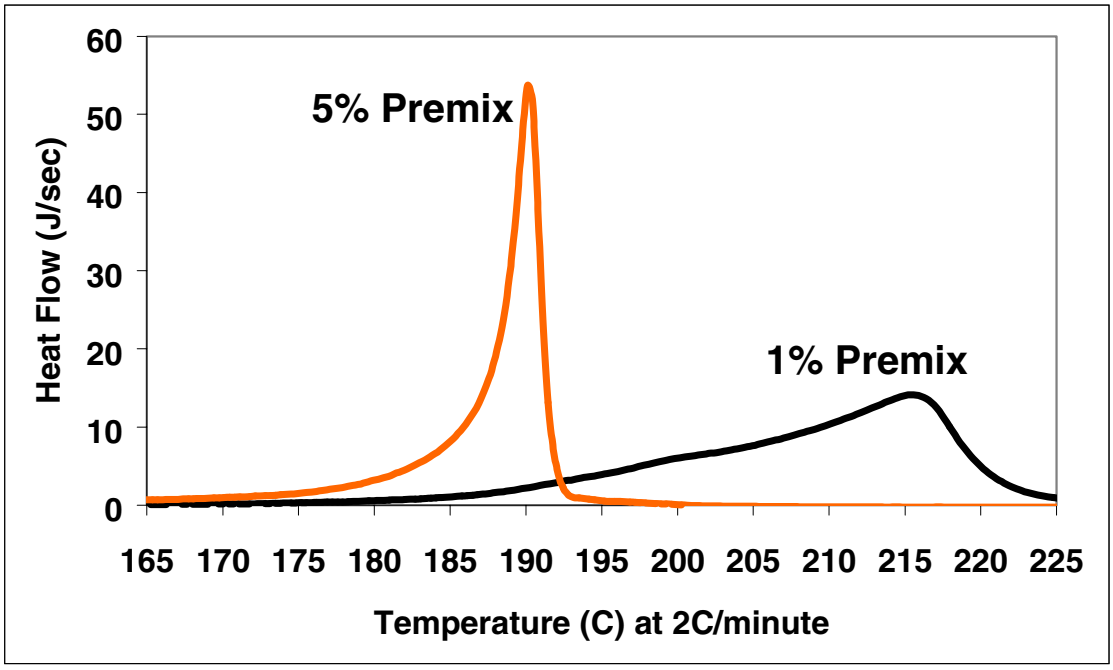

Figure 3 DSC results for epoxy monomer with 1% and with 5% clay at 2°C/minute

The increase of nanoclay concentration in the resin premix was confirmed to reduce the maximum reaction temperature. This trend was best seen at 5°C/minute as shown in Figure 5.

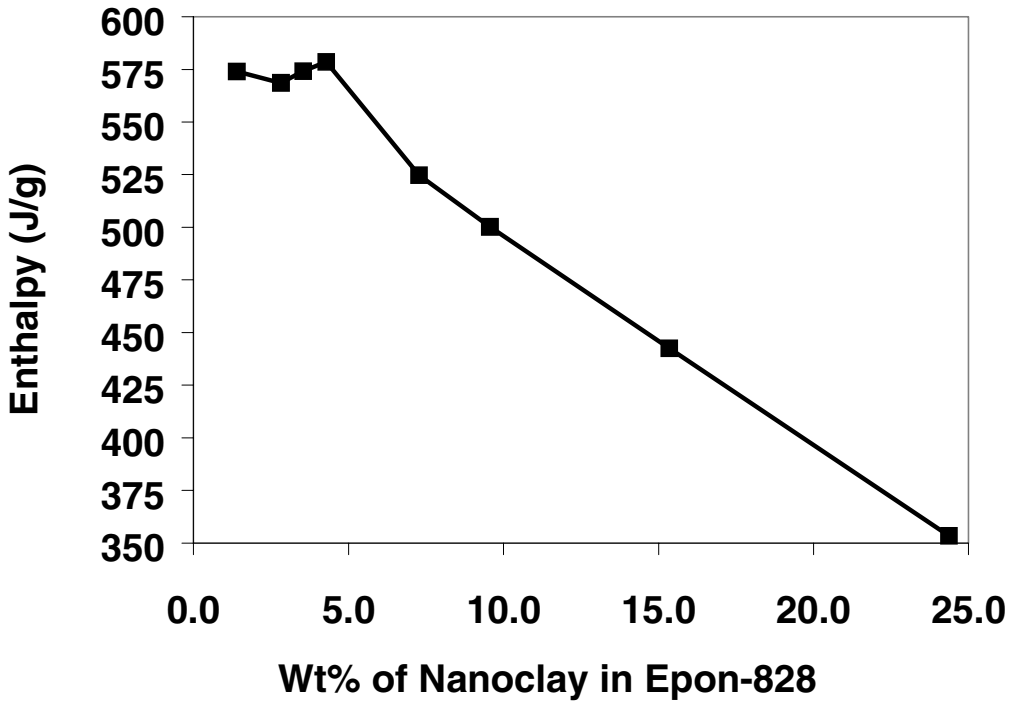

Figure 4 Enthalpy of self-polymerization of Epoxy at 5°C/minute

A more extensive series of DSC tests was required to examine the three-part mixture. Non-isothermal kinetic determinations were selected to reduce the amount of time required for test. This approach requires a minimum of three different constant heat rates. The constant heat rates of 2, 5, and 10°C / minute were used to investigate both kinetic as well as diffusion effects on the epoxy polymerization reaction that might change due to clay concentration. Shifts in the temperature of the peak maxima and the

shape of the exotherms were similar with clay concentration at each constant heating rate. Differences in the enthalpy results were most clearly resolved in the test results for 2°C/minute as shown in **Figure 5**.

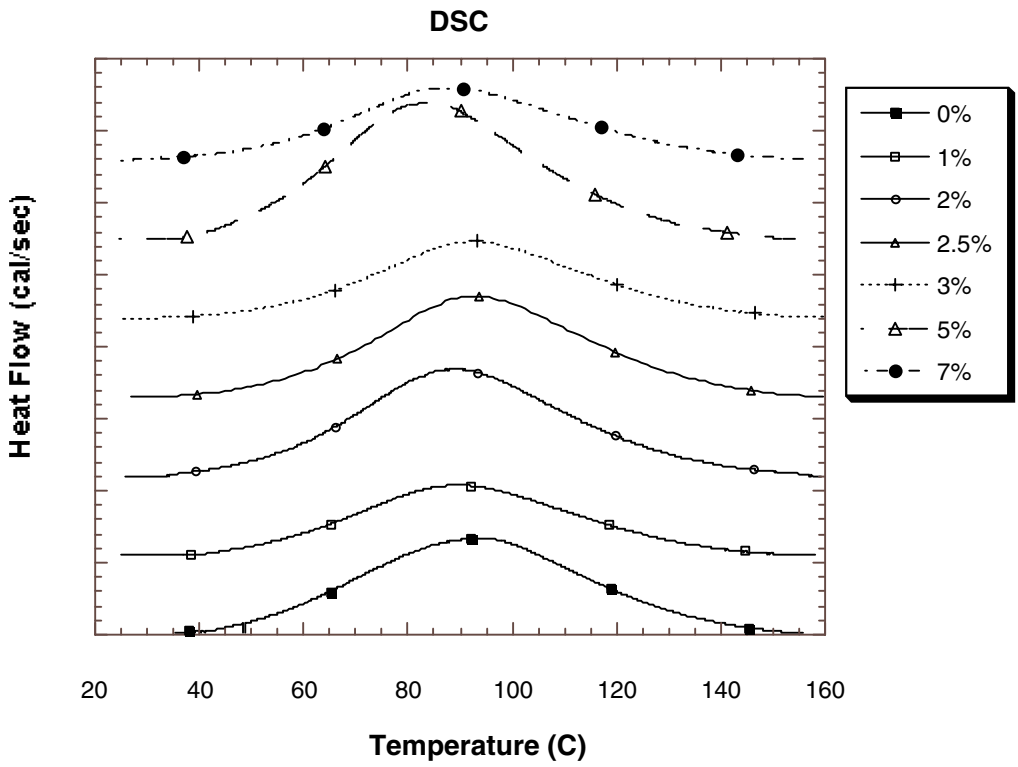

Figure 5 Concentration effects of clay on the enthalpy of 3-part mixtures.

The kinetic analysis was performed on the three-part mixture according to the ASTM method (39). If a diffusion effect should appear then molecular hindrance would be found to affect the chemical reaction. This is explained below in terms of the Arrhenius frequency factor. An increase in the reaction peak temperature of the

exotherm at each heat rate was observed. The peak temperatures were plotted as a function of heating rate. The results were fitted to the Arrhenius relationship given by **Equation 9**:

Equation 9

$$k = Ze^{\left(\frac{-E_a}{RT}\right)^n}$$

Where:

Z = pre-exponential factor

E_a = activation energy in J/mole

R = 8.3144 ideal gas constant in J/(mole K),

T = Temperature in degrees Kelvin

n = Reaction order

The application of **Equation 9** begins by a determination of the reaction order (n). This quantity is a constant found by the general rate law. The general rate law may be explained as a plot of the cure function against its time first derivative for different constant heat rates.

Equation 10

$$\frac{dC}{dt} = k(1-C)^n$$

Where:

C = cured fraction

t = time

n = reaction order (Fit indicates n =1; i.e. first order reaction)

The temperature (T_{max}) where the maximum reaction rate was observed at each of four constant heat rates was used to construct straight line plots of ln(heat rate / /T_{max}^2) versus (1 / T_{max}). The slope of this line is the activation energy, and discrete values of these slopes are plotted as a function of nanoclay content as shown in **Figure 6.** The error in the activation energies represents the goodness of fit among the four heat rate data points used for each calculation. This error is small however the graph indicates difficulty in estimating a difference in the activation energy parameter based on the effect of clay concentration.

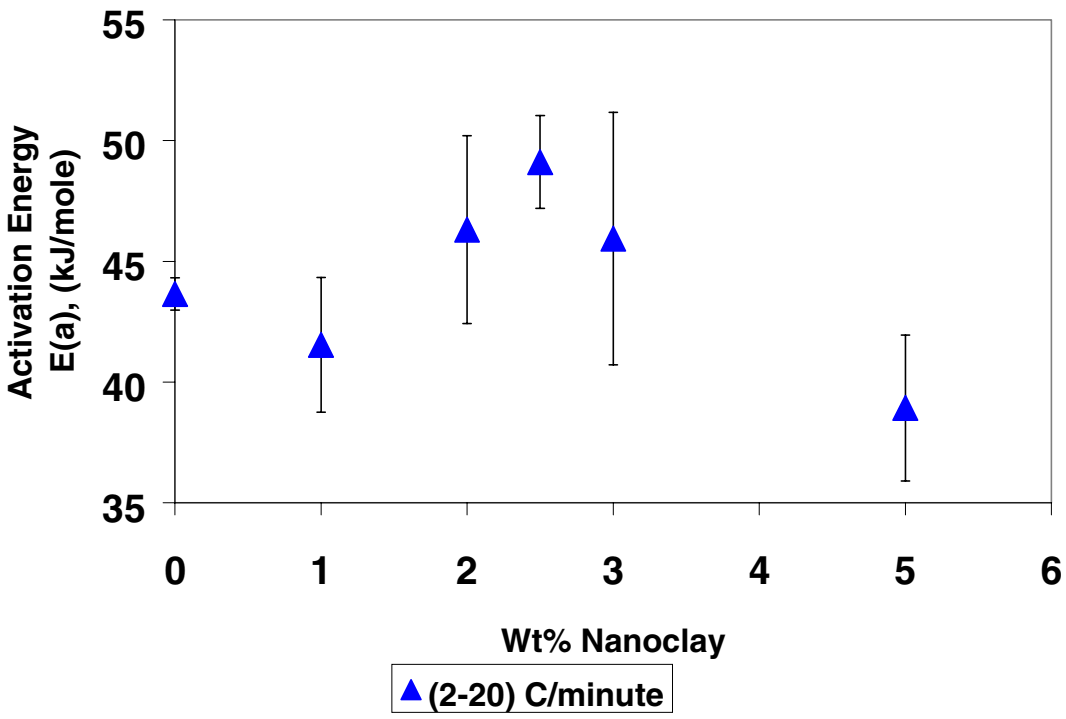

Figure 6 Activation Energy for cure of Epon 828, Nanoclay, and amine hardener

The pre-exponential or frequency factor (A) was found from the activation energy and the temperatures of the maximum reaction rate according to **Equation 4** and adjusted by a factor of 1.052 to correct for non-isothermal kinetics. This correction is according to

the general method for polymeric reactions (40) and has been applied to reactive polymers with nanoclay (7):

Equation 11

$$A = \frac{\frac{dT}{dt} E_a e^{(E_a / RT)}}{RT^2}$$

Where:

dT/dt = heat rate, in °K / minute

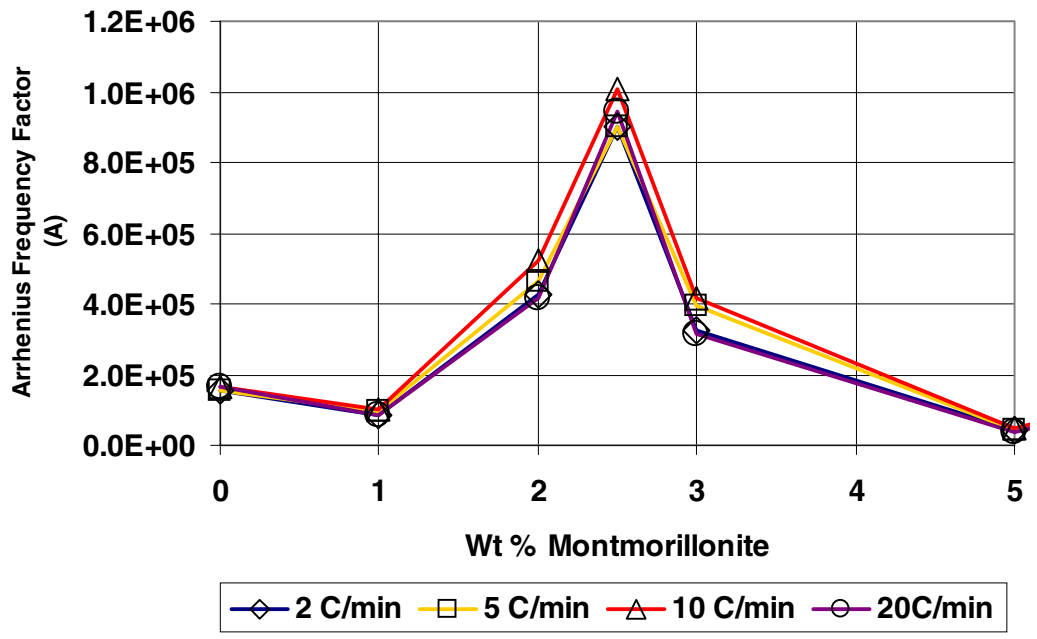

Figure 7 **Arrhenius frequency factor for the cure of three-part mixtures.**

Independence of the Arrhenius frequency factor plotted **Figure 7** from the heat rate of test shows the rate of cure was not limited by diffusion of epoxy and hardener through the nanoclay on a molecular level. This indicates each reactant was labile, or had

sufficient energy to be free to move at each test temperature. The frequency factor used to calculate this effect can be explained by quantum mechanics. A time lag for the reaction might be observed even though the energy to go from products to reactants has not been altered. At any given constant temperature, a given population has a distribution of reactants that have a certain level of energy. Only those molecules that express sufficient energy at a given moment can overcome the activation energy barrier to react. When only a small amount of reactant molecules possess this energy in a given population, then the probability is that it will take a long time for some of them to attain the correct energy state. If the temperature is increased, this increases the probability of finding more reactants in the desired reactive state. The frequency factor is therefore a constant that expresses that population of reactants ready to react.

As can be seen the presence of the clay may have changed the apparent activation energy somewhat. A more sensitive test to determine changes in the reactivity as a function of concentration is to record the temperature of the maximum rate of the reaction as shown in **Figure 5** for concentrations of nanoclay.

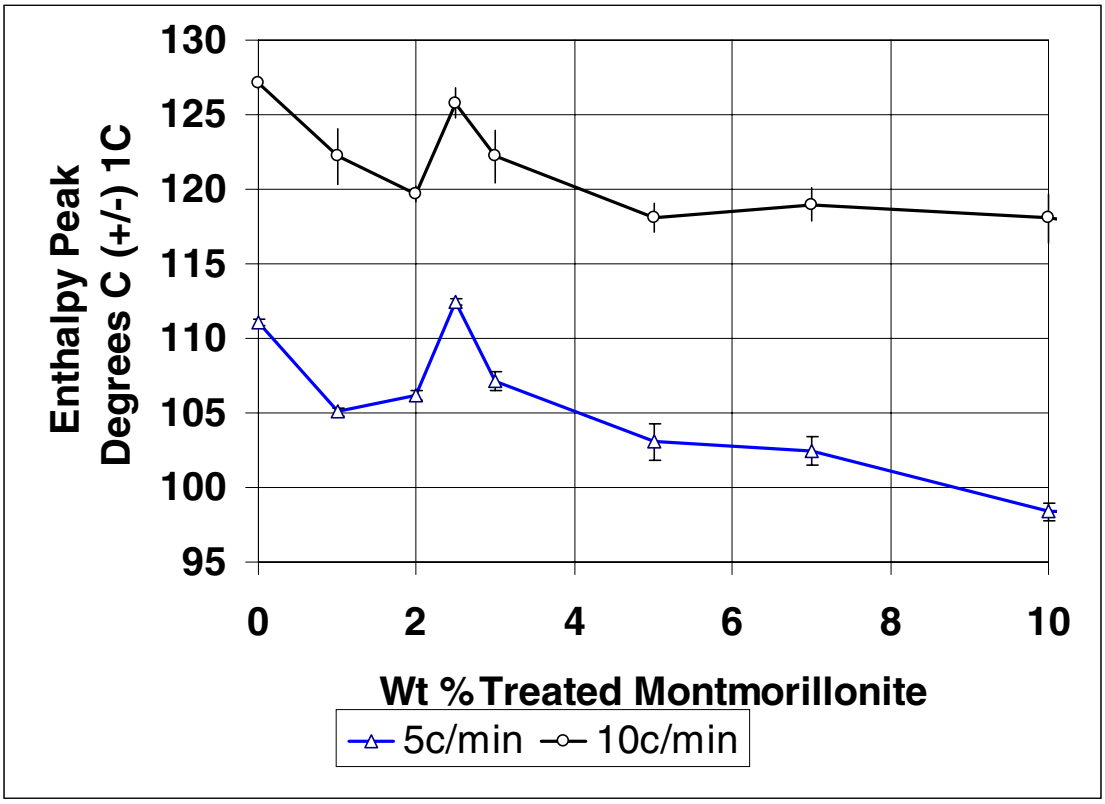

Figure 8 **Concentration effect on exotherm temperature for cure of three-part mixtures**

Alteration in reaction temperature is a matter of concern not only for the manufacture of the nanocomposite, but because any change may thermally and therefore entropically destabilize the favorability of the reacting polymer to remain dispersed between the clay platelets.

CHAPTER 5

MICROSTRUCTURE

5.1 X-ray diffraction

Nanocomposite X-ray diffraction results attest that either exfoliation or intercalation dispersion of nanoclay was successful in each cured panel. X-ray diffraction for the nanoclay is compared to that for the reacted composite specimens in **Figure 9.**

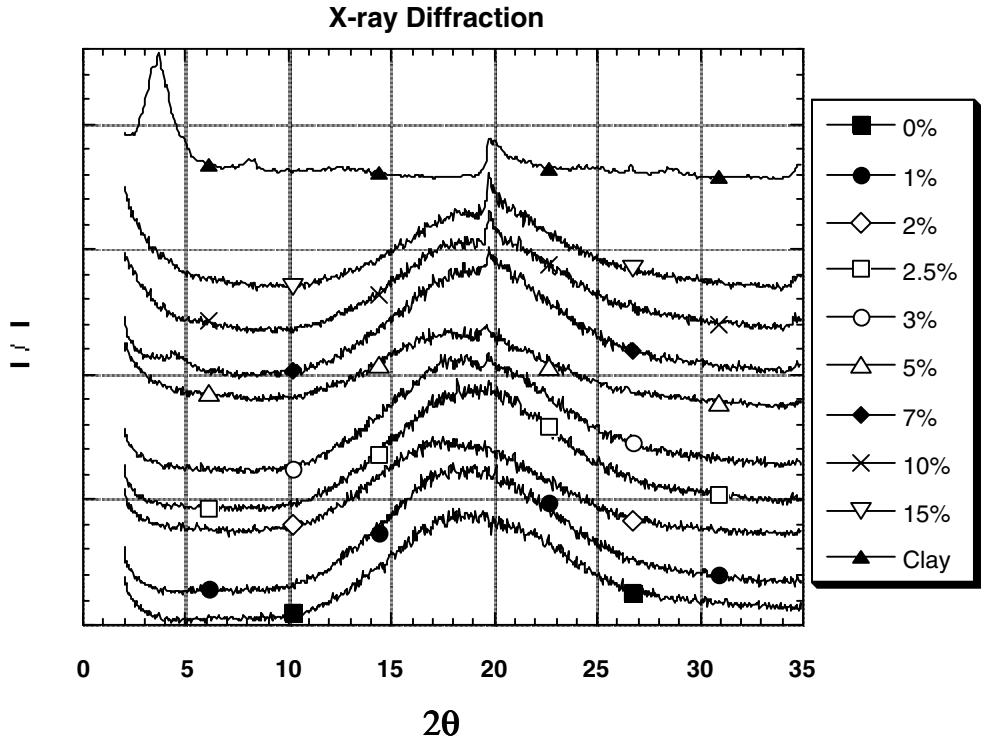

Figure 9 X-ray diffraction spectrum of treated clay compared with cured nanocomposite.

The x-ray diffraction of the treated montmorillonite clay shows the 001 silicate crystal lattice plane reflection at $2\theta = 3.65^{o}$ that corresponds to the interlayer spacing of the regular stacked nanoclay structure by use of the Bragg equation for diffraction:

Equation 12

$$n(\lambda) = 2d \sin \theta$$

Where:

d = distance between silicate lattice planes that are parallel

θ = Incident angle of the x-ray to the lattice plane

λ = The wavelength of x-ray used for this analysis, 1.54056 Å

n = some number of wavelength periods

The meaning of the combined term (d sin θ) may be thought of as the correct distance between two x-rays that happen also to be the correct angle of incidence for a constructive interference to occur between these waves. The physical significance of the d-spacing is shown by the silicate structure in **Figure 10.**

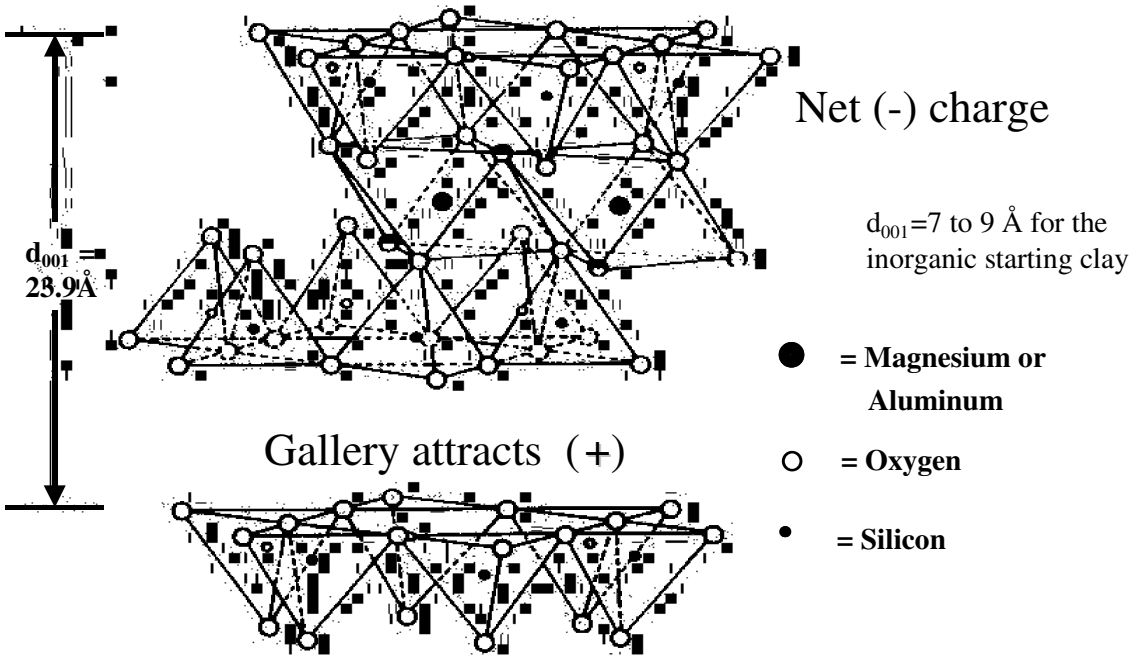

Adapted from *Suspensions: Fundamentals and Applications in Petroleum Industry*, L.L. Schramm, American Chemical Society, Washington, D.C. (1996).

Figure 10 Physical significance of the d_{001} spacing to the intercalated structure.

Since the angle of incidence is known, and the wavelength is known, a trigonometric relation of the sine function (opposite / hypotenuse) allows the distance between the reflecting planes to be calculated. If a crystal has d-spacing that correspond to a repeating lattice of points, the smallest unit of that separation in 3-space may be denoted as (a, b, c). The reciprocal of the unit cell spacing is the miller index d (*h, k, l*) most commonly used to denote which of many possible reflections is being referred to.

Examination of the x-ray (001) reflection in the diffraction of all the nanocomposite panels at 2θ of 2 degrees is shown in **Figure 11**. This indicates that the degree of dispersion into polymer was best for the nanoclay at less than 3% by weight, but still dispersed well for each of the 1% to 15% clay and epoxy mixtures even after consideration of possible detrimental effects mentioned earlier in reference to the chemical reaction.

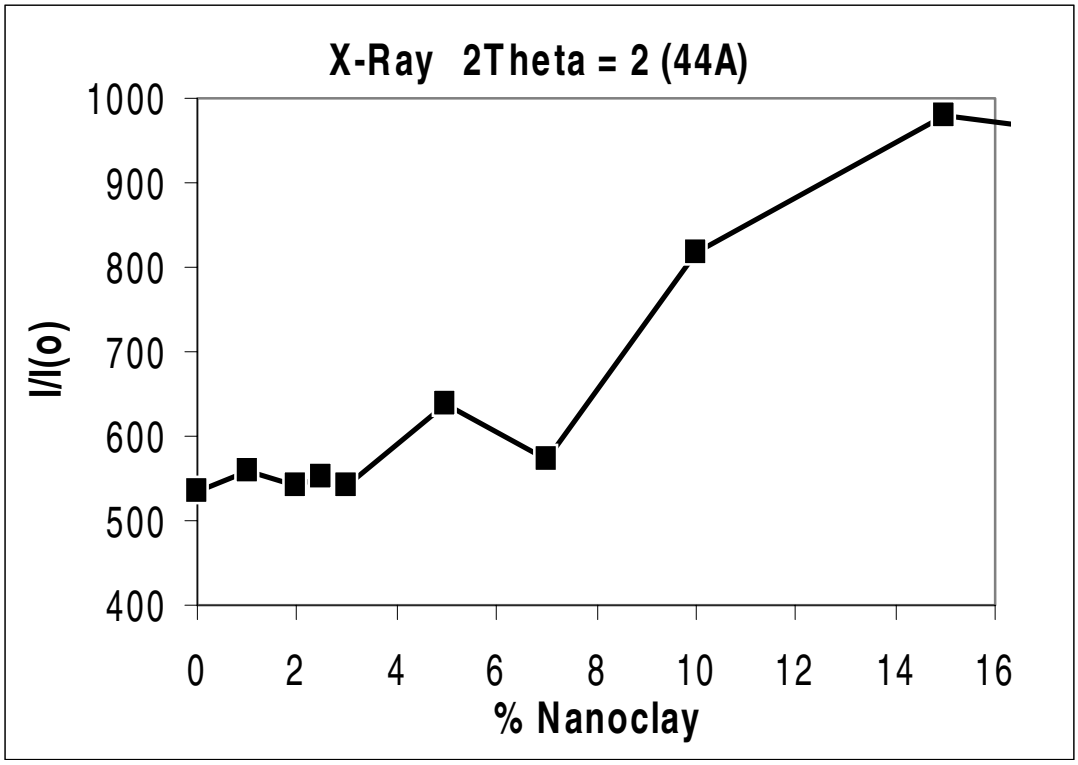

Figure 11 **X-ray diffraction between parallel surfaces of the Silicate platelets at 44 Å**

The overall or long-range structure of the clay platelets was adequately resolved in most cases by SEM, and supplemented by exact knowledge of the local structure and dispersion of each clay platelet by TEM. Large-scale structure probably results from the

both the increased packing of the clay and a probably self-organizing charge orientation effect. Orientation seems reasonable to expect for particle interaction at elevated concentrations due to a charge balance packing mechanism expressed by the clay platelets.

5.2 SEM

Each SEM micrograph discussed below was obtained from the fracture surface of a tensile specimen that was mounted onto an aluminum stage and vapor-deposited with gold to permit microscopic imaging of the sample.

The microstructures obtained from these SEM micrographs indicated there was not a simple order of structure versus nanoclay concentration. There were three distinct regions of clay platelet morphology. In the first, round clusters predominated. In the second, a flat layered structure predominated. Finally there was third region characterized by no long-range microstructural order. One of the regions of no long-range structural order was observed to exist between two clearly defined structures. These regions were best understood by examination of the trend in each microstructure that occurred from the well defined state characterized by the round and then the flat structures found at either end of the range of concentrations examined. The low concentration regime was examined first to understand the effect of increase in the amount of nanoclay on the globular structure. The high concentration regime was then examined to understand the effect of a decrease in concentration on the laminar structure. The probable identity of the regions where the clearly defined regimes ended could then be inferred by a consistent extrapolation of each trend.

The low concentration range begins with amorphous epoxy polymer with 0% clay additive. This pure epoxy had a dramatic broken brittle failure fracture pattern shown in **Figure 12** typical of cured epoxy that has failed below T_g. This brittle fracture pattern is commonly referred to as the chevron pattern due to the repeated fracture shape.

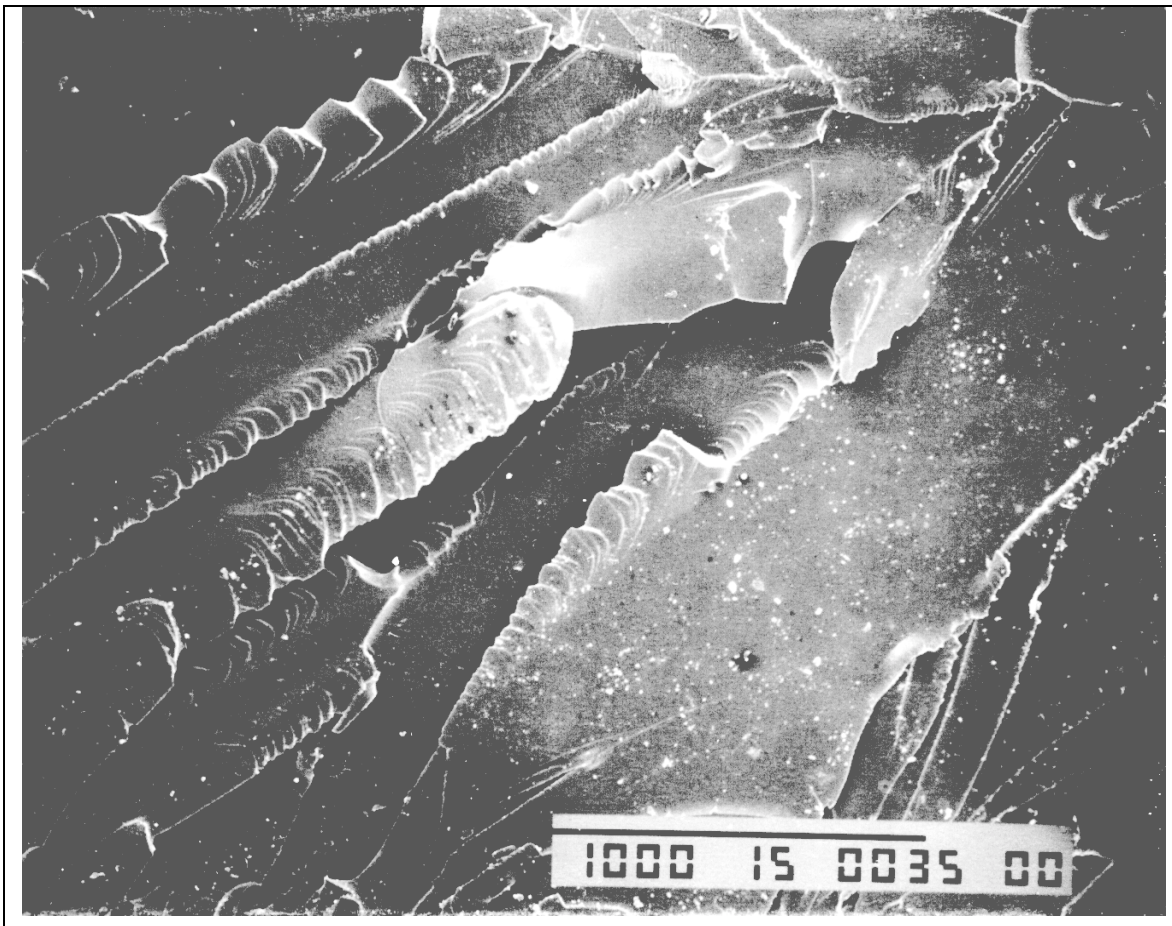

Figure 12 0% montmorillonite tensile fracture surface of cured epoxy at 35-X

This "chevron" pattern is visible at higher magnification as seen for the glassy microcrack that progresses from the upper left to the lower right corner of the micrograph of cured epoxy at 0% clay shown in **Figure 13**.

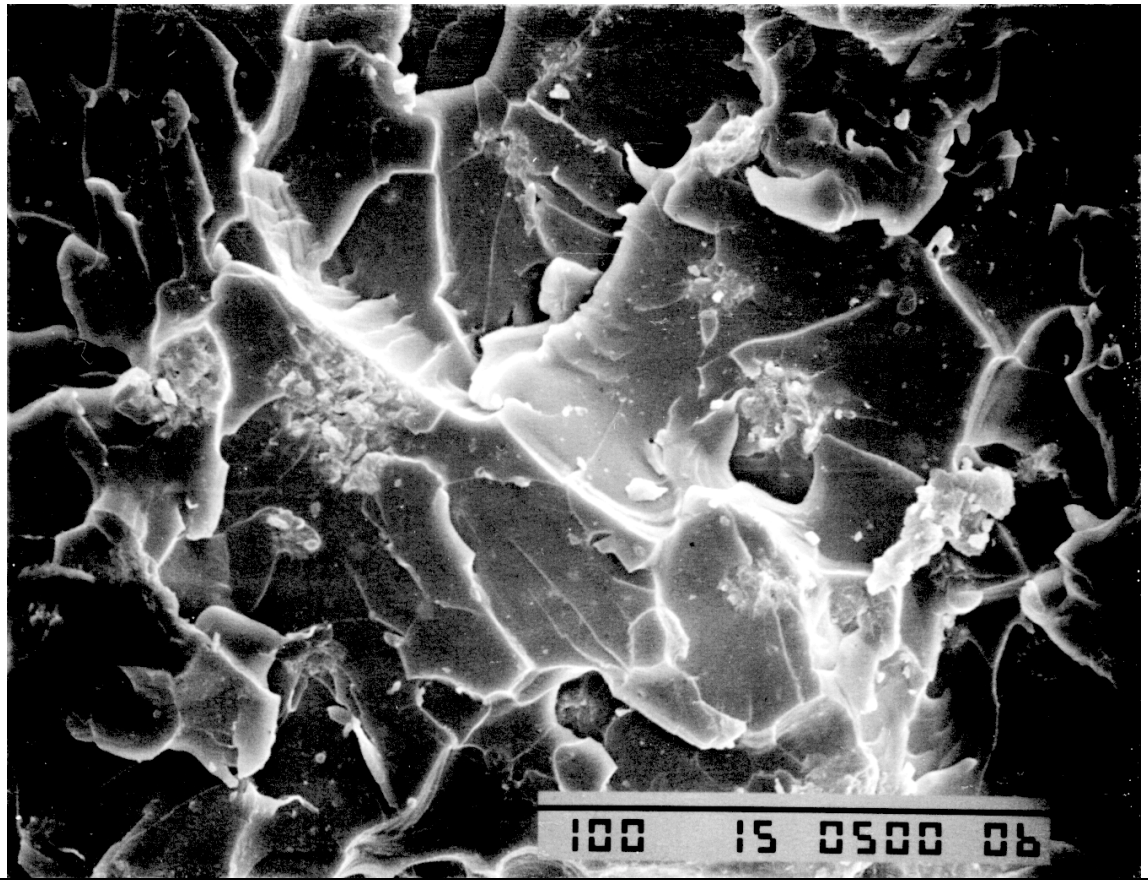

Figure 13 0% montmorillonite cured epoxy at 500-X magnification

On the addition of 1% of nanoclay, the silicate platelets orient into small round micelle-analogs. **Figure 14** indicates the amount of jagged glassy surface features have been reduced dramatically, but not eliminated. The overall nature of failure appears to have changed due to the various sized round clumps of nanoclay that appear to be pulled out of the fracture surface in this SEM micrograph. Some evidence of random glassy failure might still be found in the diagonal crack surface from center to the lower left corner.

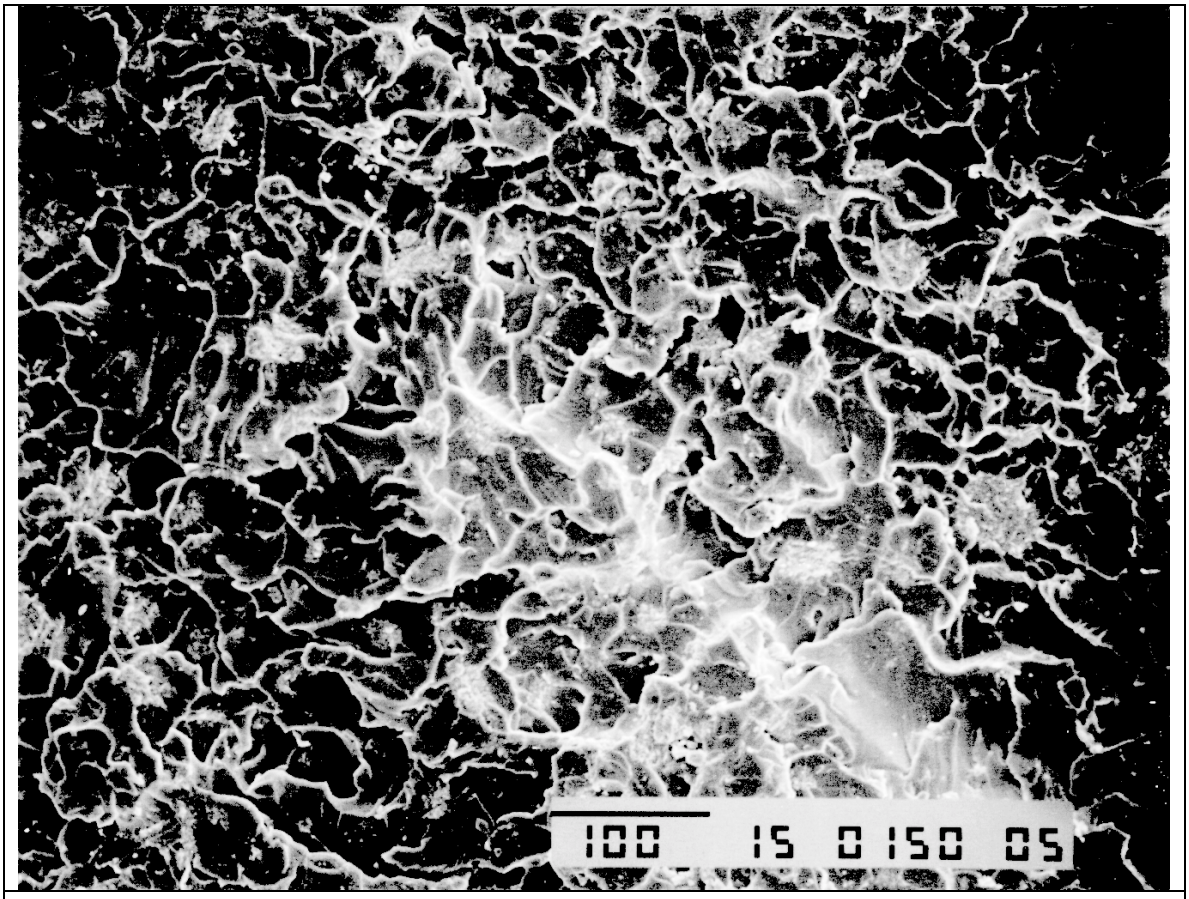

Figure 14 **1% montmorillonite at 150-X magnification**

Figure 15 shows the form of random out of plane tears that extend from the initiation of the crack for 2% clay in cured epoxy. This is evidence of ductile deformation, however higher magnification is required to help determine if there is a microstructural explanation for this observation.

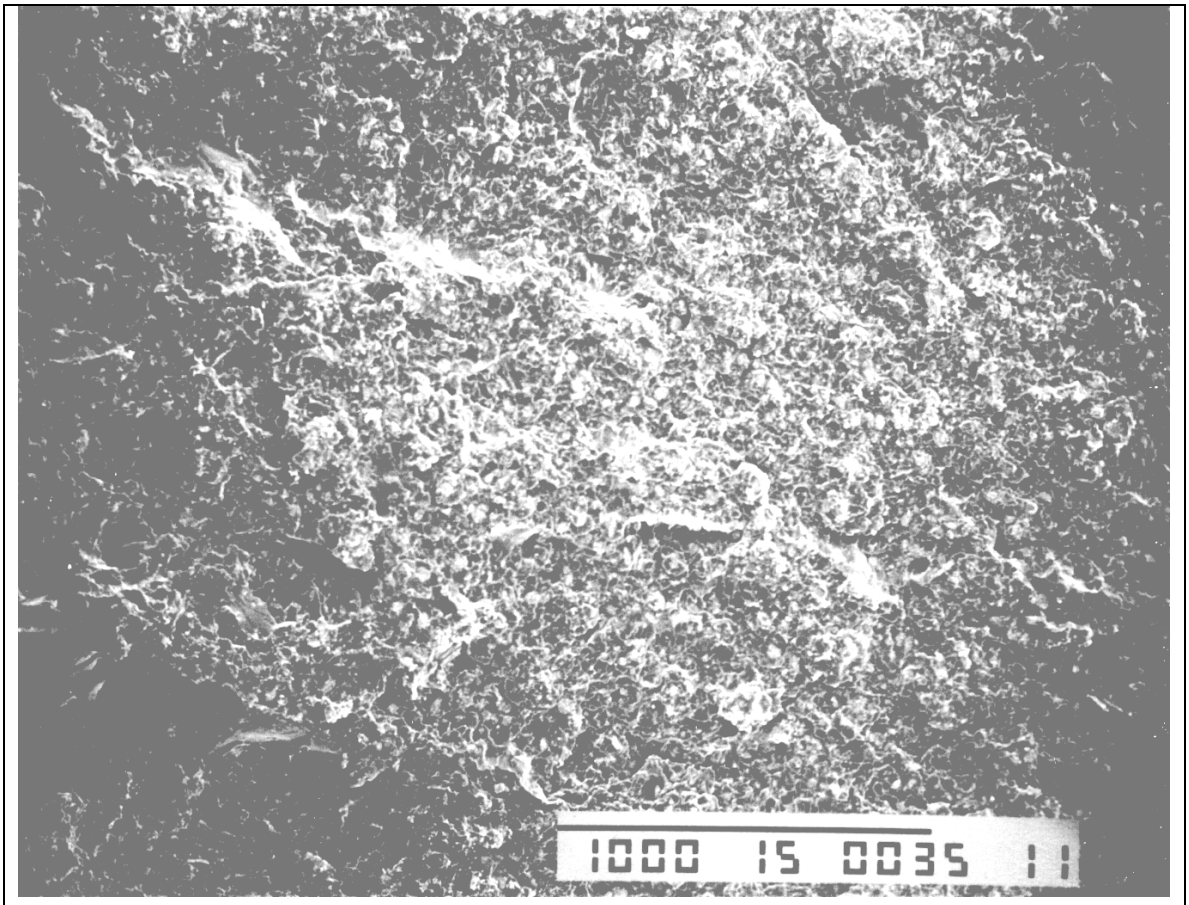

Figure 15 2% montmorillonite fracture surface at 35-X magnification

The reason for the tearing ductility is shown in **Figure 16**. Many spherical clay agglomerates of differing diameters appear at the site where the ductility was observed. This microstructure explains the local evidence of ductile failure. The particle clump at the lower center was worthy of a closer view to capture the way the crack initiation has resulted in this overall structure.

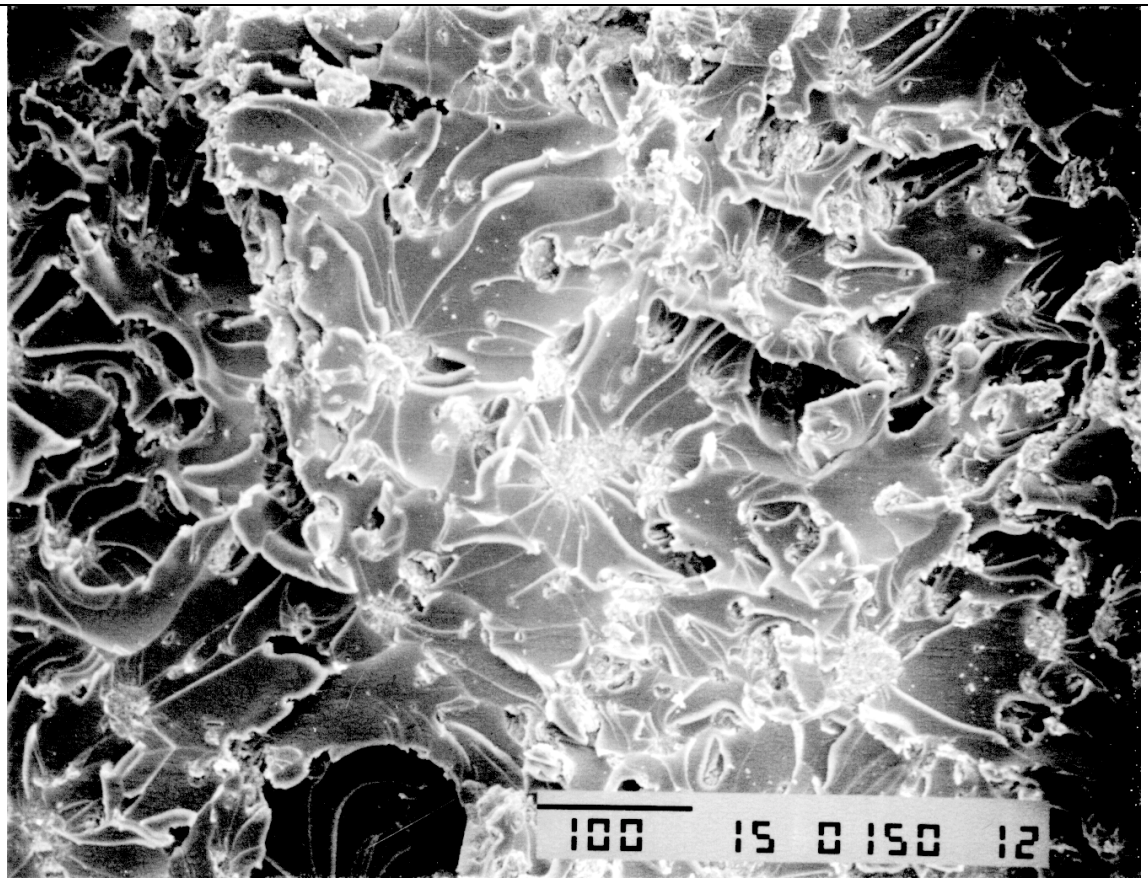

Figure 16 2% montmorillonite fracture surface at 150-X magnification

Figure 17 shows a magnified view of the elongational shear in the epoxy around a micellar region. The large area of the epoxy fracture surfaces can be seen. This indicates local ductility around the particle at the crack initiation point at 2% clay concentration. The increase in fracture surface area available to absorb energy is the correct kind of indication for improvement in impact resistance and ductility.

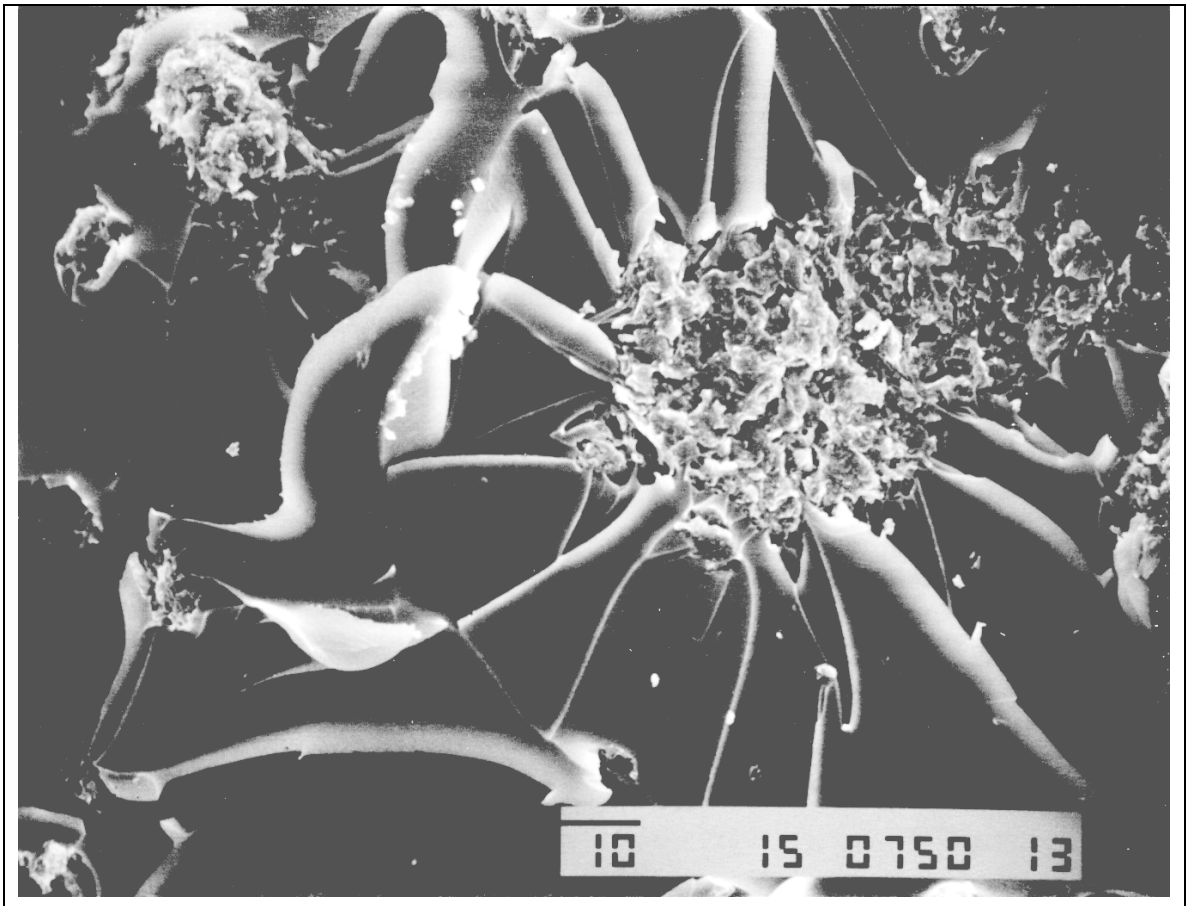

Figure 17 2% montmorillonite fracture surface at 750-X magnification

The SEM micrograph of 2.5% clay in **Figure 18** at 150X demonstrates the apparent mechanism of ductile reinforcement. Here, the spherical clay agglomerates have been dragged along through the epoxy to form long tubular paths at the initiation of the crack. This is an important observation because the means of generating brittle matrix brittle reinforcement toughening strategies can be pictured with this concept in mind.

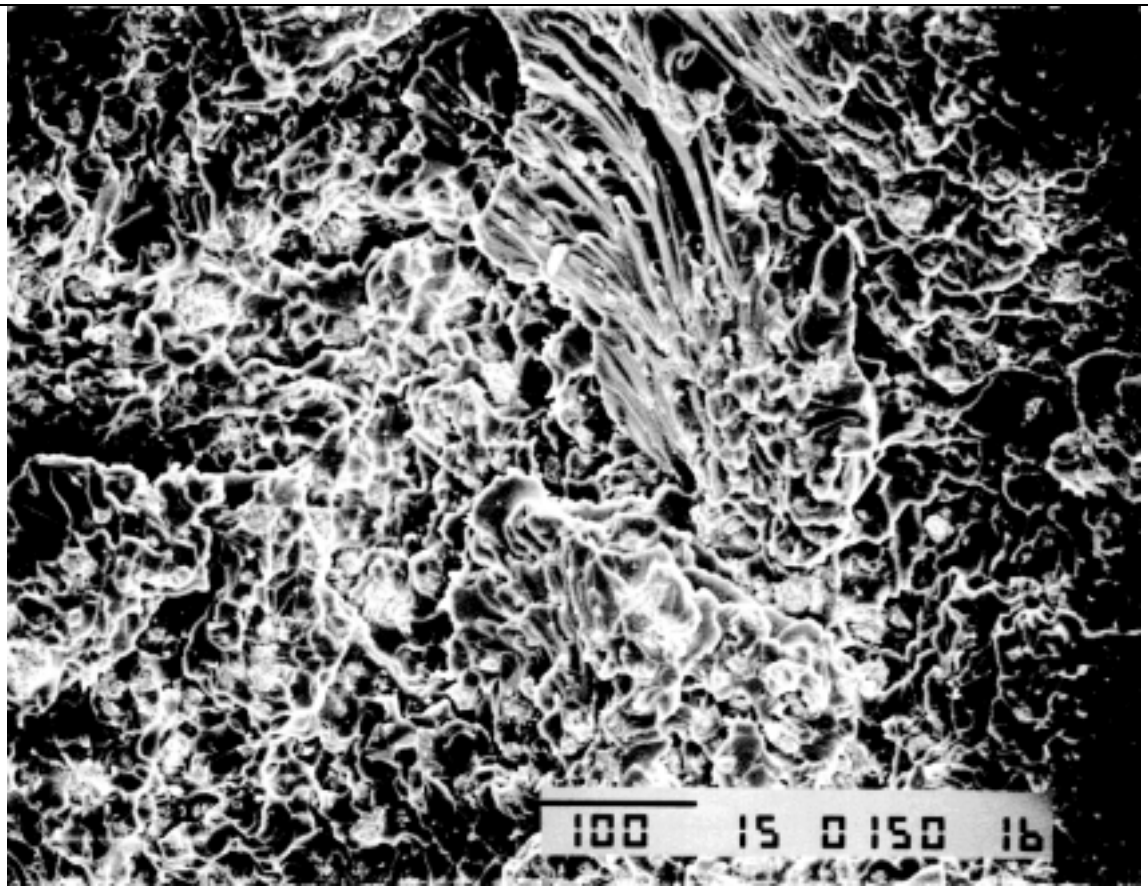

Figure 18 2.5% montmorillonite fracture surface at 150-X magnification

The increase in both the size and the range of diameters of the spherical clay agglomerates at 2.5% concentration is the most likely explanation for the increased properties found at that concentration. The number and distribution of spherical clay agglomerates appears to have reached its peak at 2.5% nanoclay, as suggested by **Figure 19**, where 5, 10, and 20 micron clay agglomerates have not yet flocked to join their larger cousins that were observed at the lower magnifications. A systematic study of the size and distributions of these particles is recommended.

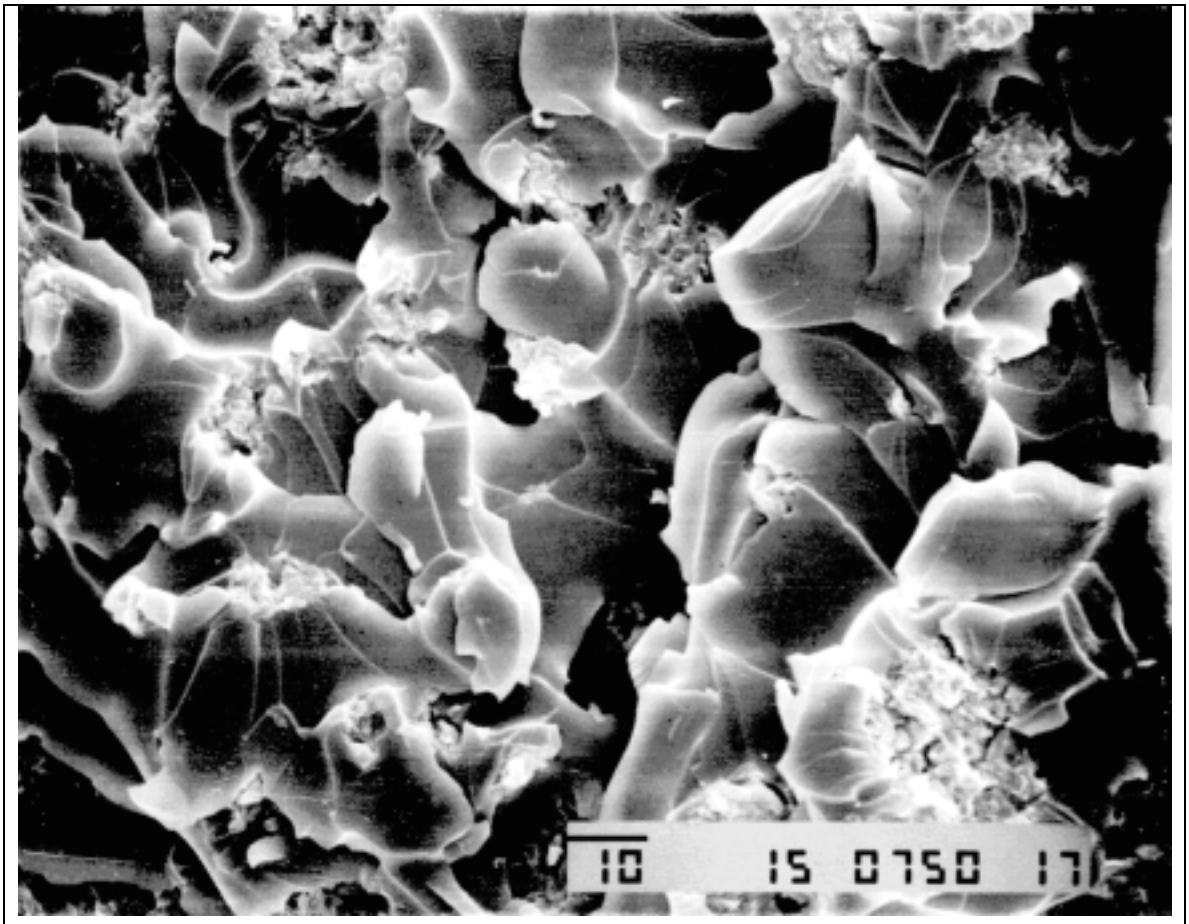

Figure 19 2.5% montmorillonite fracture surface at 750-X magnification

A concentration of 3% nanoclay showed reduced indications that sufficient charge isolation was present for spherical clay agglomerates to form at 30 microns. Large clay agglomerate structures were not visible at this nanocomposite concentration. Once again the occurrence of a common microvoid was able to indicate a clearer example of the dominant morphology seen in other views of the pulled out structures. Here a spherical clay agglomerate was found isolated inside a microvoid shown in **Figure 20**.

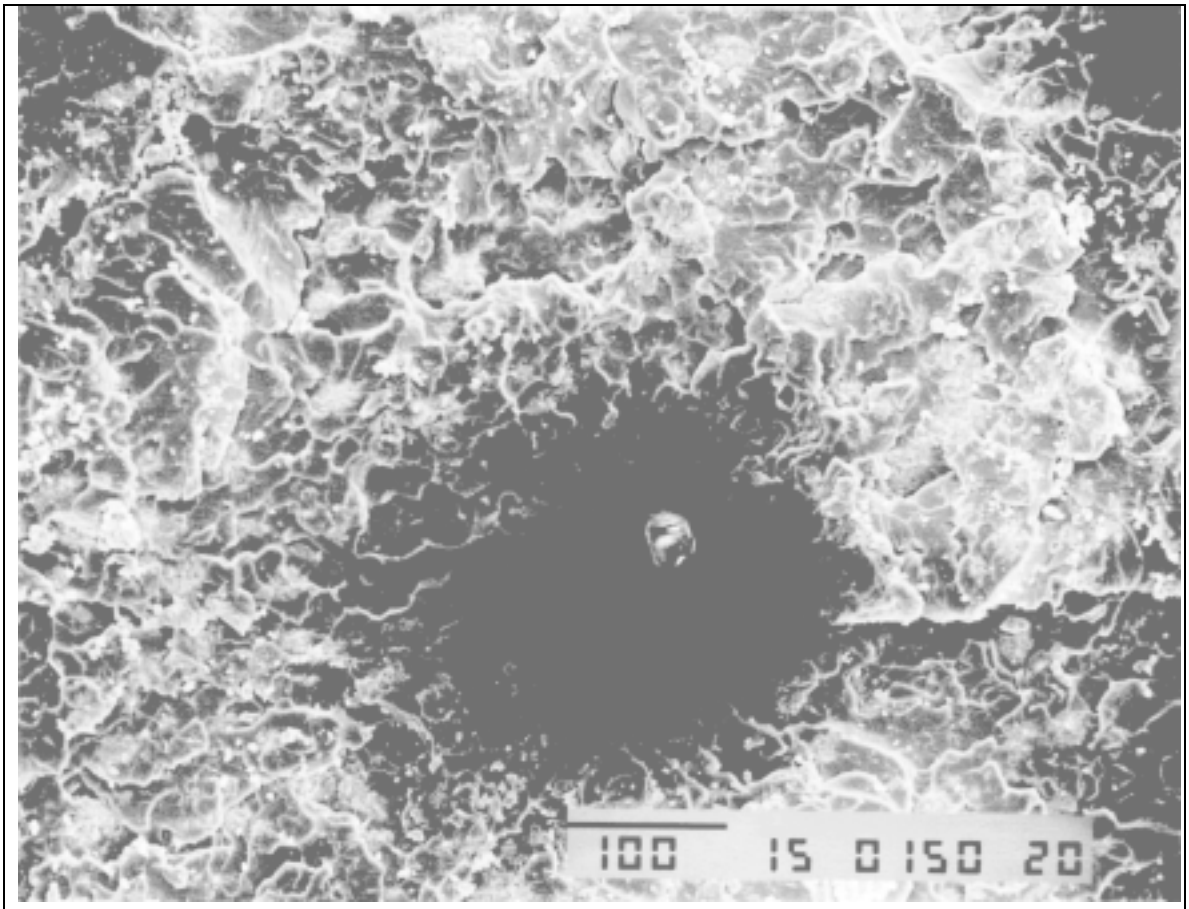

Figure 20 3% montmorillonite clay void inclusion at 150-X magnification

A direct comparison of the particle in **Figure 20** with the particle of **Figure 26** illustrates the difference of the two kinds of shapes that the clay particles may form. At 3% nanoclay the return to some kind of particle inclusion yielded a return to a ductile mode of failure as shown by the raised regions of about 30 microns diameter due to spherical clay agglomerates seen in **Figure 21**. These particles are of much smaller diameter and appear to be more widely dispersed at 3% nanoclay than was the case for the 2.5% clay previously discussed.

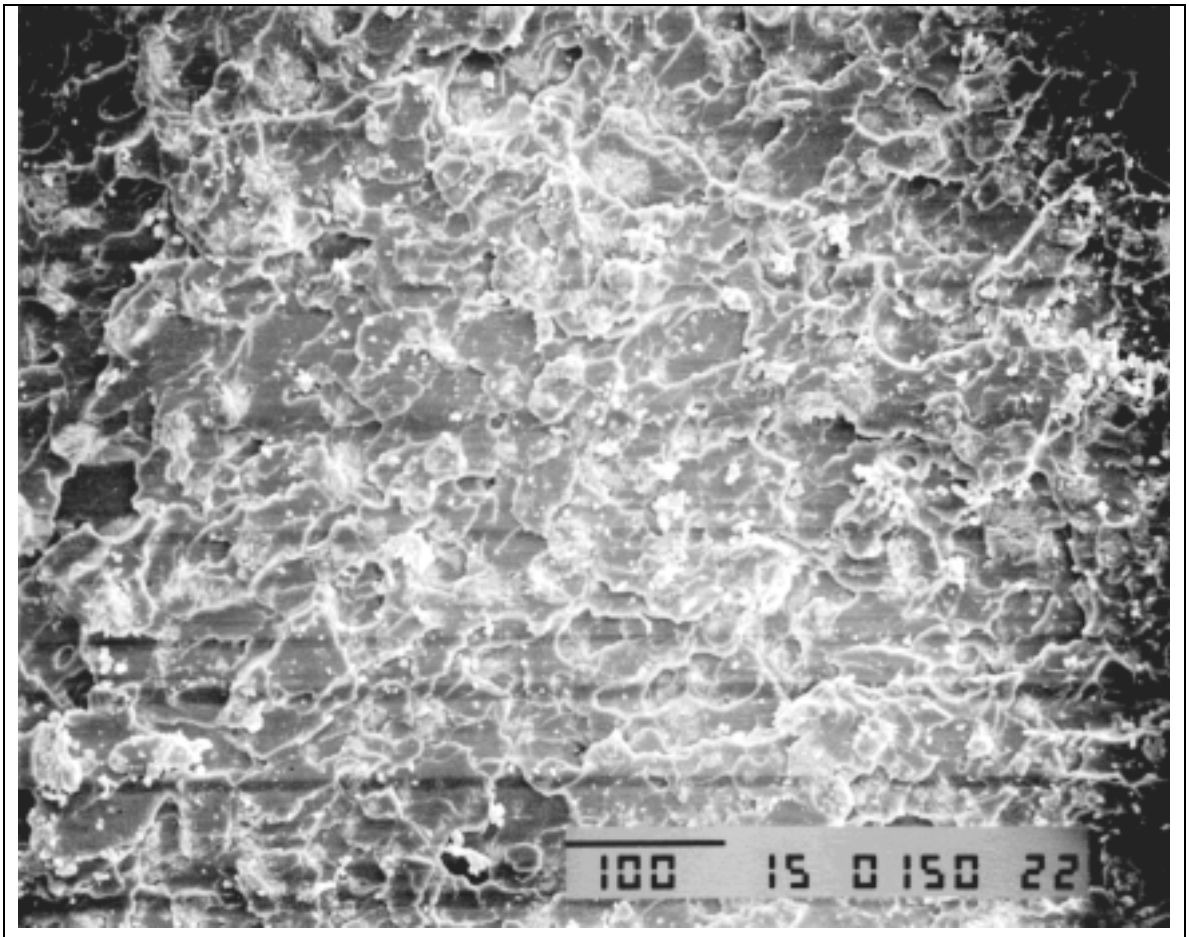

Figure 21 3% montmorillonite fracture surface at 150-X magnification

The concentration at 5% nanoclay is below that required to form layers, as shown in **Figure 22.** Interestingly there are no flocks or micellar regions in this view, which indicates these types of structures are either not present in quantity or are not favored for this concentration. The type of failure shown is brittle failure, and this view at the initiation of the crack.

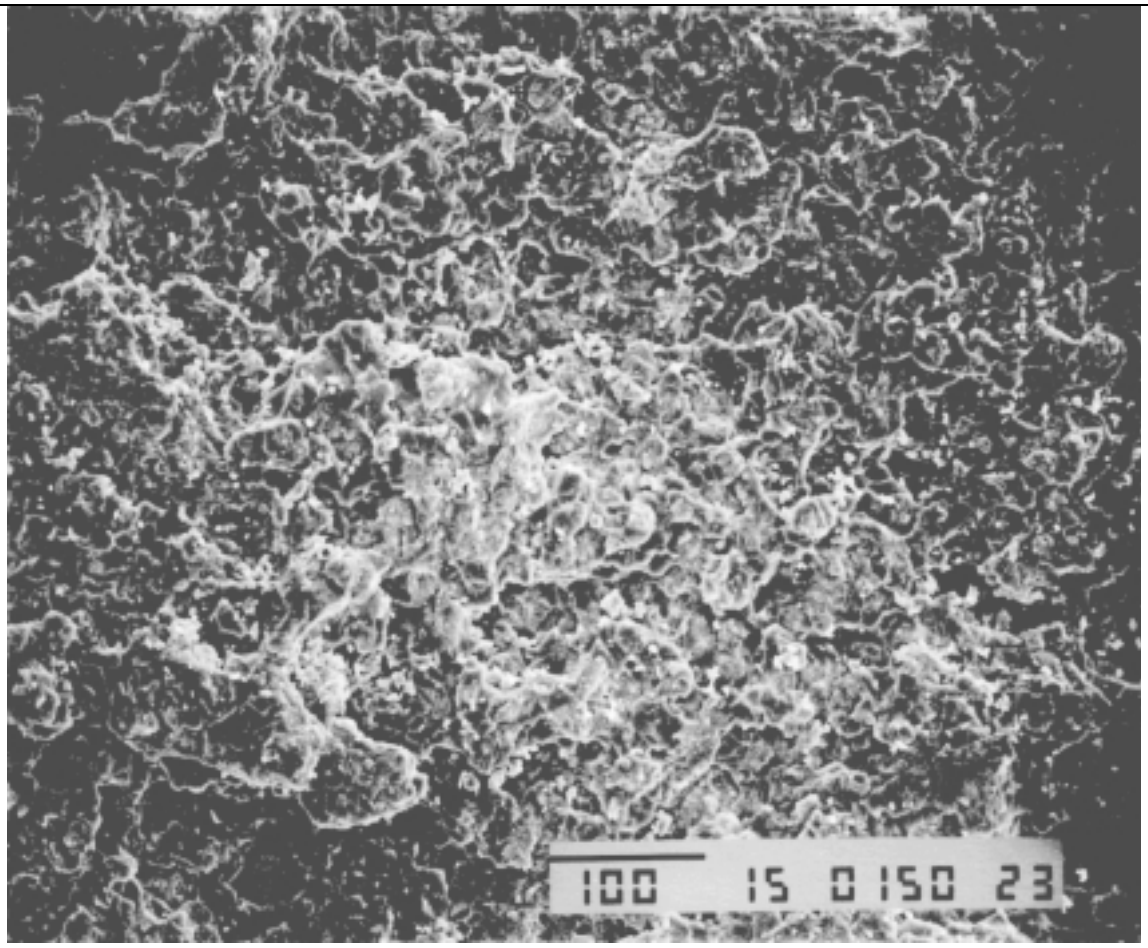

Figure 22 5% montmorillonite fracture surface at 150-X magnification

The randomness of the crack among the exposed surfaces in **Figure 23** signals a return to a brittle failure mode and a three dimensional state of stress. The 5% concentration therefore signaled arrival at some intermediate region where no evidence of the platy or the globular structures was found. The same magnification was used as shown in the previous view, however this view is of the crack propagation region where pulled out microstructure might have appeared if it were present to do so.

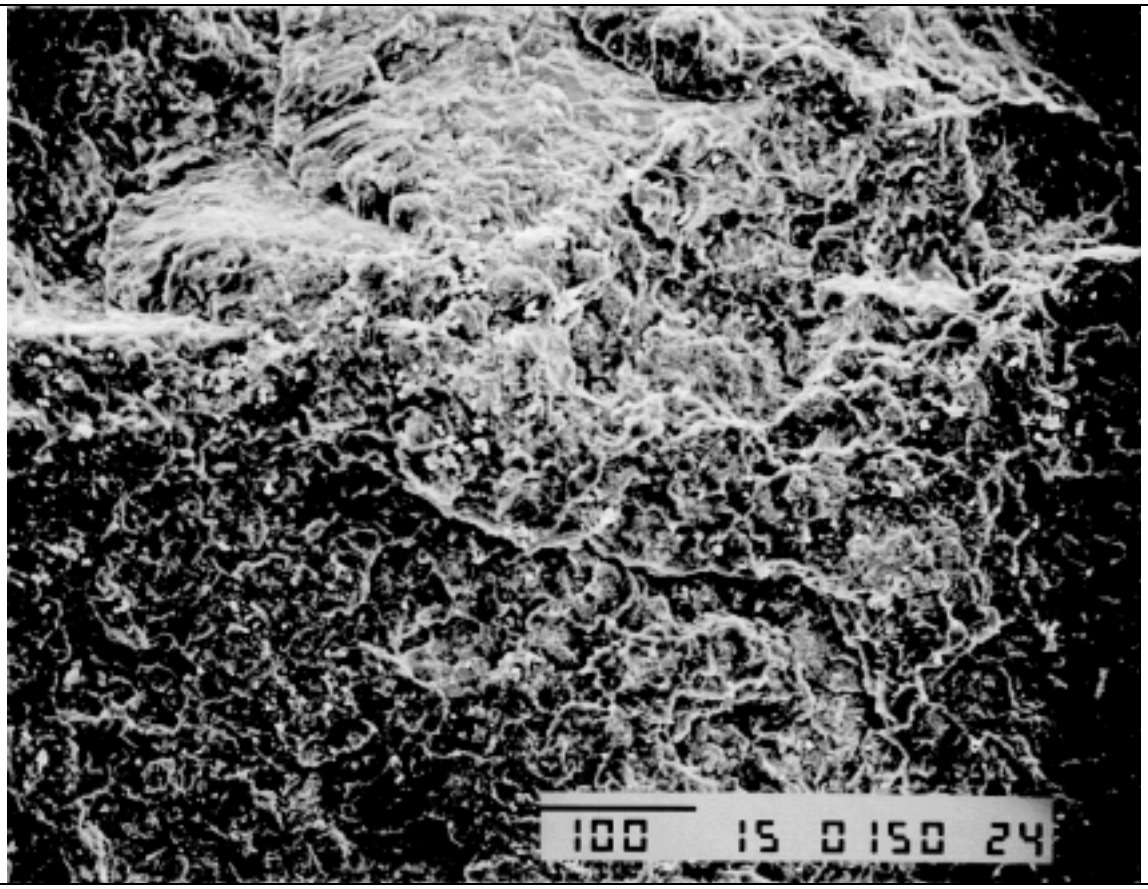

Figure 23 5% montmorillonite with crack propagation at 150-X magnification

A deviation from simple brittle coplanar failure was found with the change in concentration to 7% nanoclay. **Figure 24** demonstrates a localized three-dimensional out of fracture plane tear as evidence of the onset of ductility for the flat platy structure. This indicates that flat layers of plates of clay can also act to deform in a ductile manner.

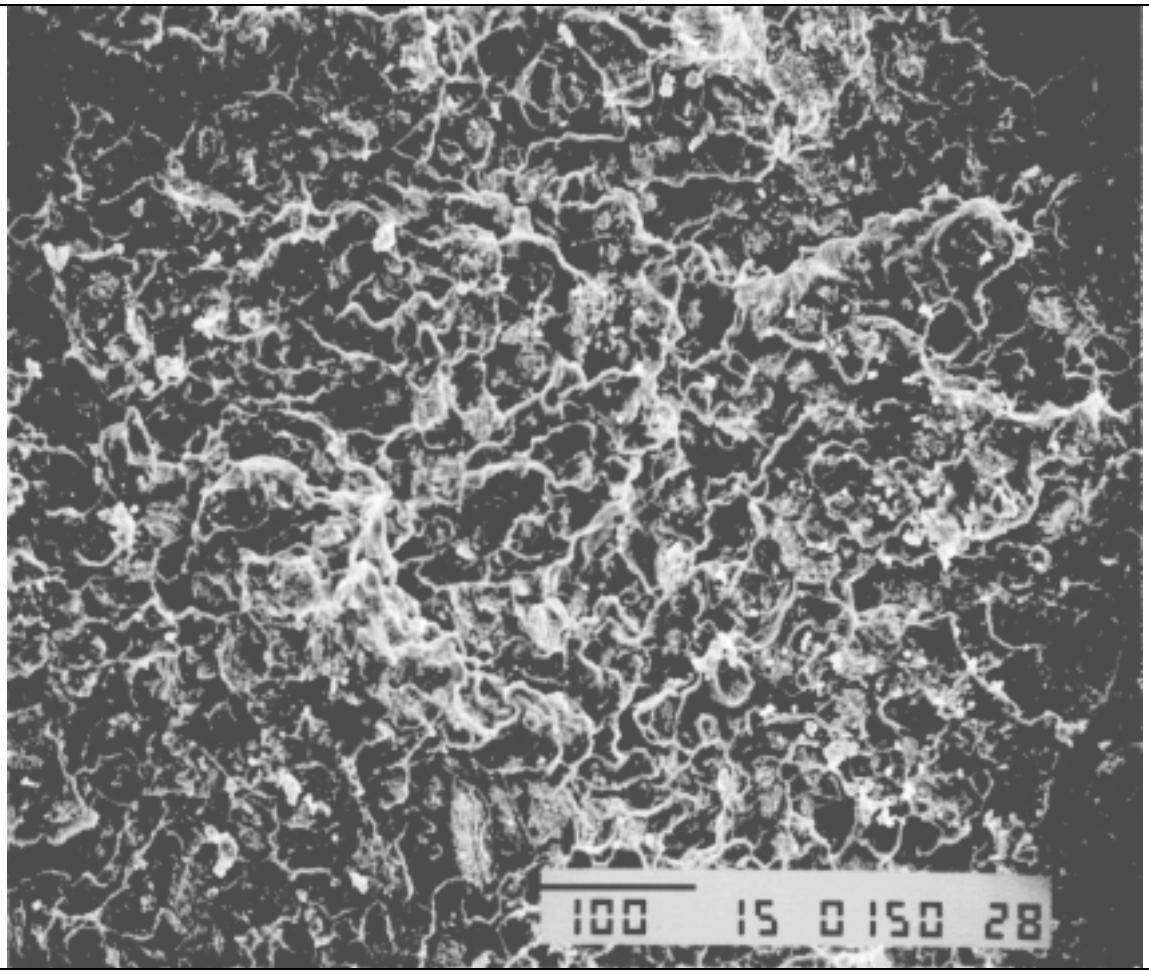

Figure 24 7% montmorillonite fracture surface at 150-X magnification

At a concentration of nanoclay of 10%, a transition was seen to the structure seen in **Figure 25** where the platelets are organized into planar layers. The type of failure was brittle failure with no evidence of ductility.

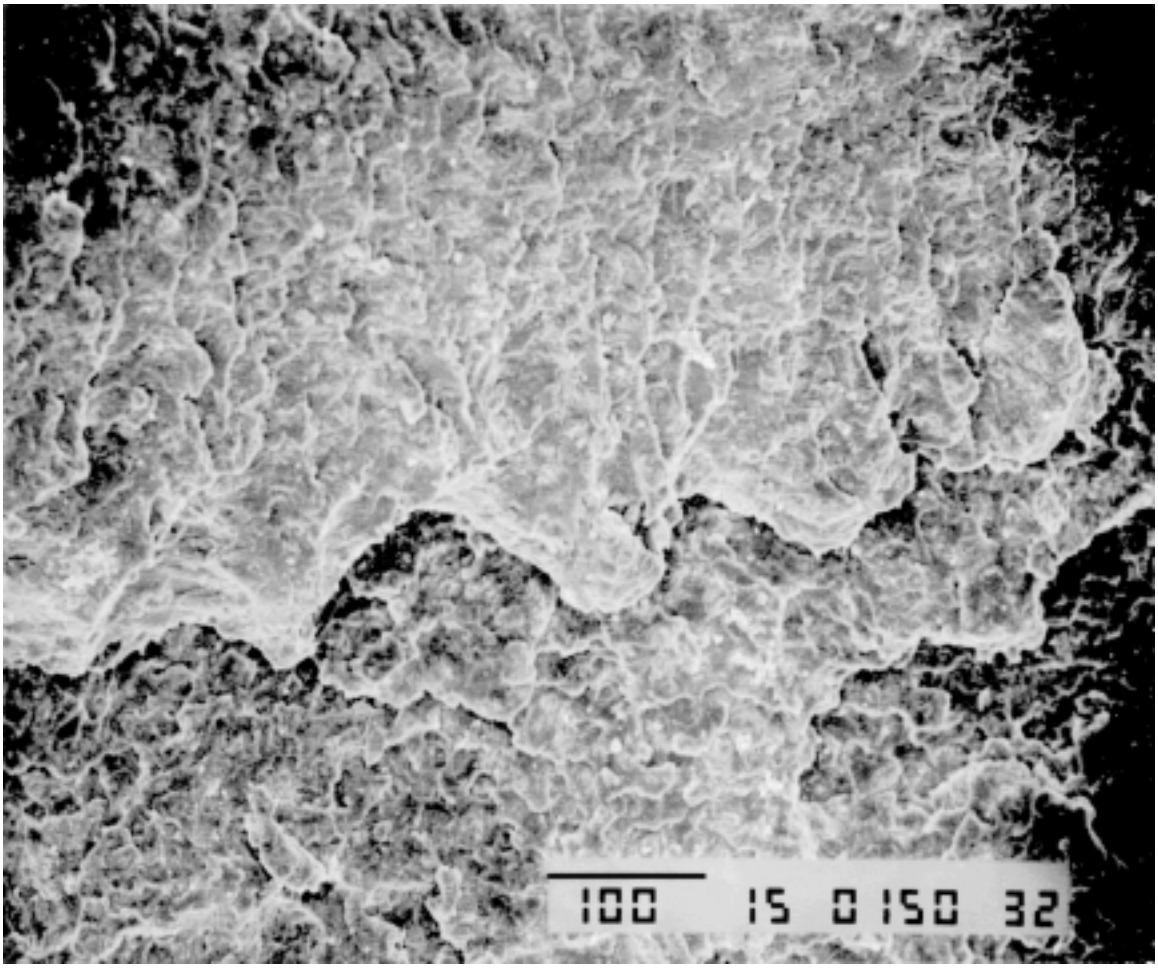

Figure 25 10% montmorillonite fracture surface at 150-X magnification

Voids are common at high clay concentrations based on the density studies described elsewhere in this work. The particle morphology at 10% clay was clarified as one layer was found in the void shown in **Figure 26**. This layer was immobilized by an entrapped air bubble that permitted observation of the structure as the void was exposed at a crack surface.

Figure 26 10% montmorillonite fracture surface at 50-X magnification

Examination at higher magnification shows the above layered structure more clearly in **Figure 27** to be composed of sheets of platelets set perpendicular to the surface of each large layer, or sheet.

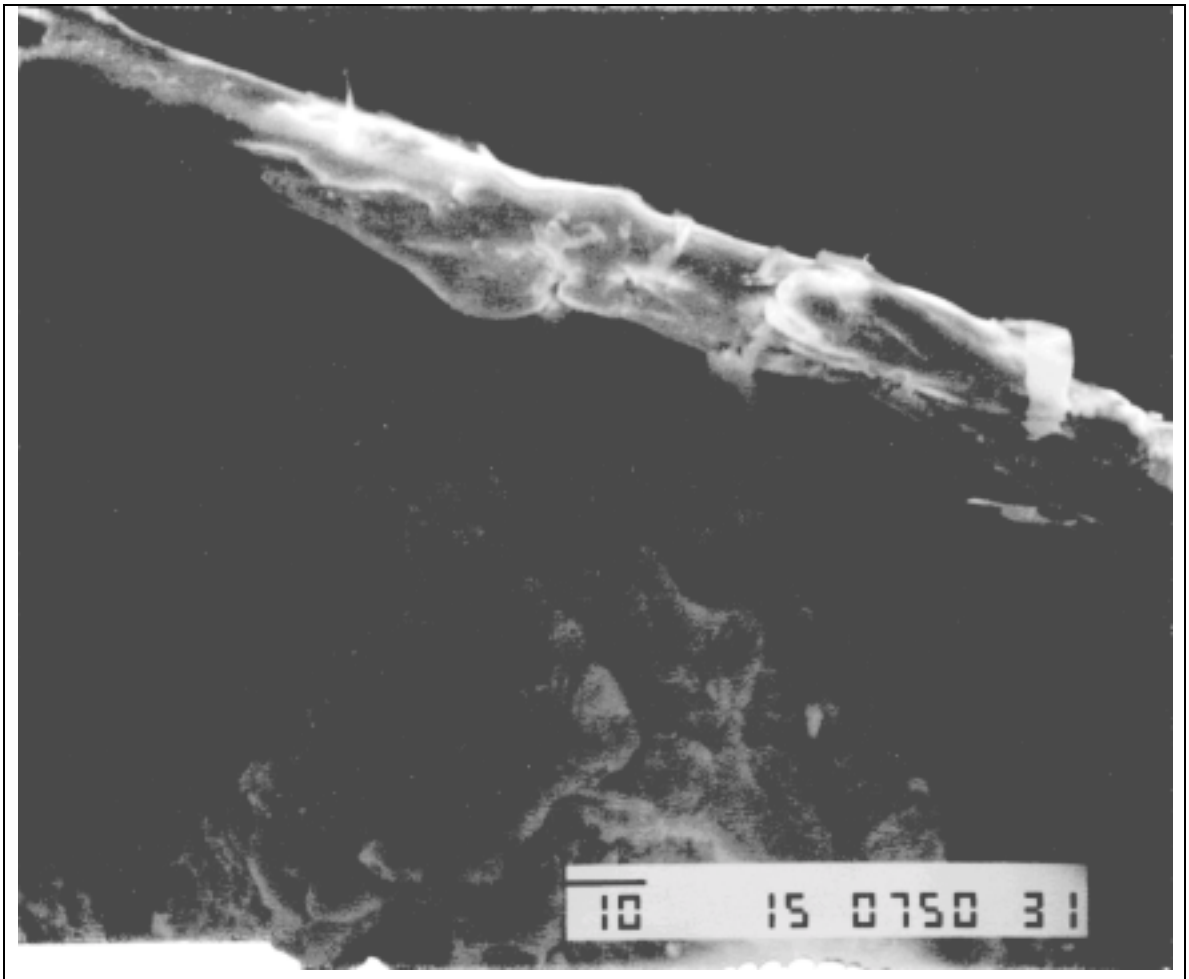

Figure 27 10% montmorillonite fracture surface at 750-X magnification

There was no appearance of layered structures at the high concentration of 15% nanoclay. **Figure 28** shows a clean brittle fracture surface that formed perpendicular to the applied tensile load.

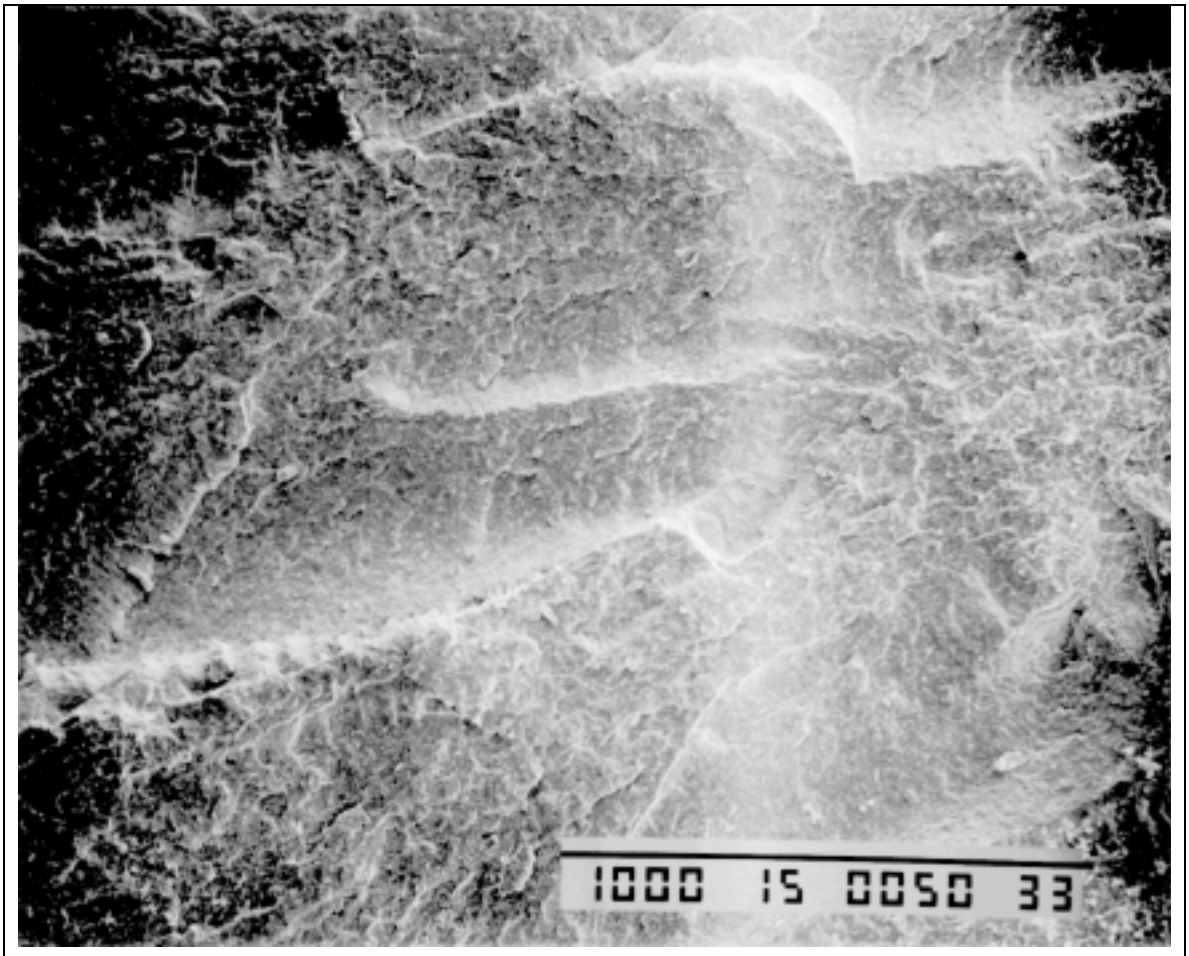

Figure 28 15% montmorillonite fracture surface at 50-X magnification

Even at higher magnification the micrograph in **Figure 29** showed no local change from brittle and coplanar failure. All particles appear uniformly dispersed with no evidence of tearing and no evidence of a layered microstructure.

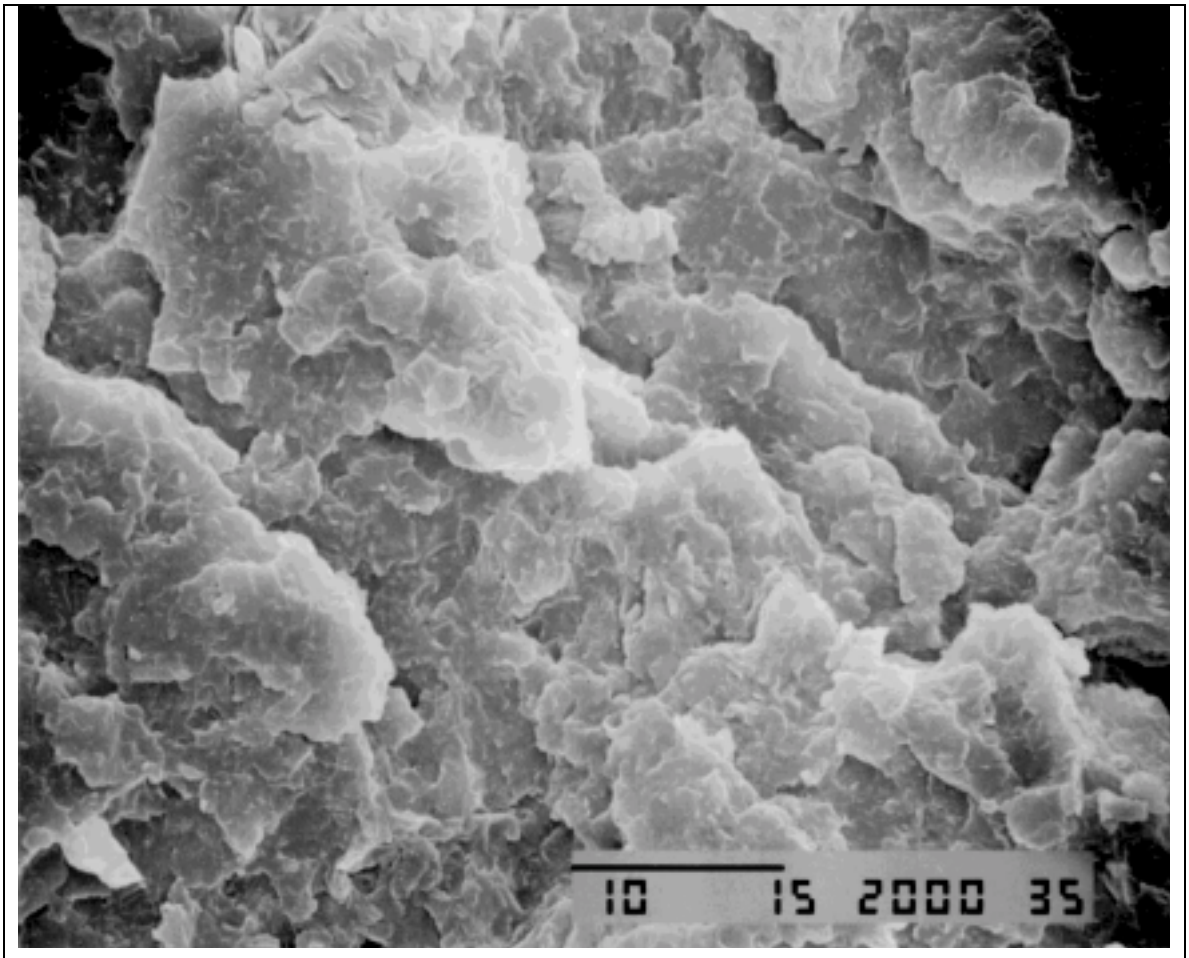

Figure 29 15% montmorillonite fracture surface at 2000-X magnification

The most significant observation brought about by the SEM analysis was the unexpected discovery of particle aggregates in epoxy nanoclay. The pretreatment of the clay was a surfactant. Surfactants are understood to form micelles at concentrations low enough to isolate small spherical regions from the mass of chemically dissimilar liquid material around it. The spherical shape serves to minimize the surface area exposed to the interface.

Kinetics of particle aggregation have been analytically expressed and summarized in the Handbook of Surface and Colloid Chemistry (41). Consideration of that work lead to the following qualitative explanations. Slow stirring such as used in this nanocomposite preparation may have favored the establishment of fruitful collisions that would result in clay particle aggregation. Energy may also have helped to overcome steric forces between individual particles. Ultrasonic treatment of the premix could have acted to speed the establishment of the equilibrium population of aggregate particles.

An examination of the trends evidenced by the microstructures at high and low concentrations indicated the least amount of ductile reinforcement was at 5% and 15% clay where no kind of particulate structure was observed. The identity of these concentrations must be a distribution of platelets that does not favor any large-scale morphology to provide reinforcement. The existence of some intermediate microstructure might explain the lack of a larger scale particulate structure. At this point the SEM analysis required additional interpretation from TEM results at far greater magnification to understand why 2.5% might form a repeatable large-scale structure and why specific concentrations may form no large-scale structures.

5.3 TEM analysis

The TEM micrograph for 2.5% nanoclay in **Figure 30** indicates the morphology is intercalated flakes of clay set roughly at a 45-degree angle where the associated platelets are oriented end-on. The dark flakes in this micrograph are more commonly referred to in the literature as tactoids. That type of herringbone structure that is shown is commonly referred to as "the house of cards" structure. The regions between the flakes that form the cards appear to be matrix epoxy that contains exfoliated nanoclays. An

explanation for the existence of the large-scale spherical clay agglomerates is suggested. A reduced concentration and edge to edge orientation appear to permit the intercalated particles to charge separate as suggested by the 45 degree angle of these tactoids. This means the opportunity for a polarized structure to form must be investigated by examination of this region at higher magnification to determine if there is an unequal nature to the clay platelet intercalation that would explain this effect.

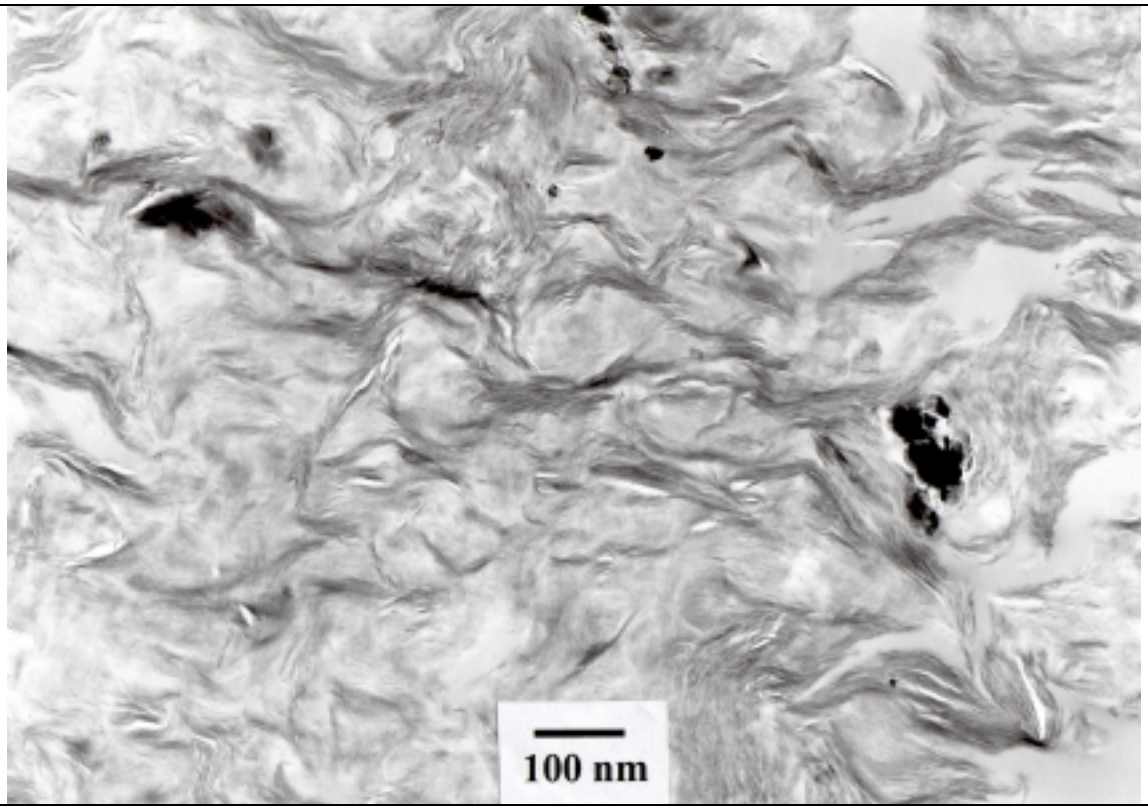

Figure 30 TEM micrograph of herringbone pattern in 2.5% montmorillonite

Figure 31 verifies a region of exfoliation where the widest spacings between clay platelets is greater than 60 nm. It can also be seen that the denser tactoid in the center is unraveling at a preferred end. It is reasonable to conject at this point that this is a cause

for charges in the clay to be dispersed over a wider area on one end of the tactoid than that part of the tactoid that is less intercalated.

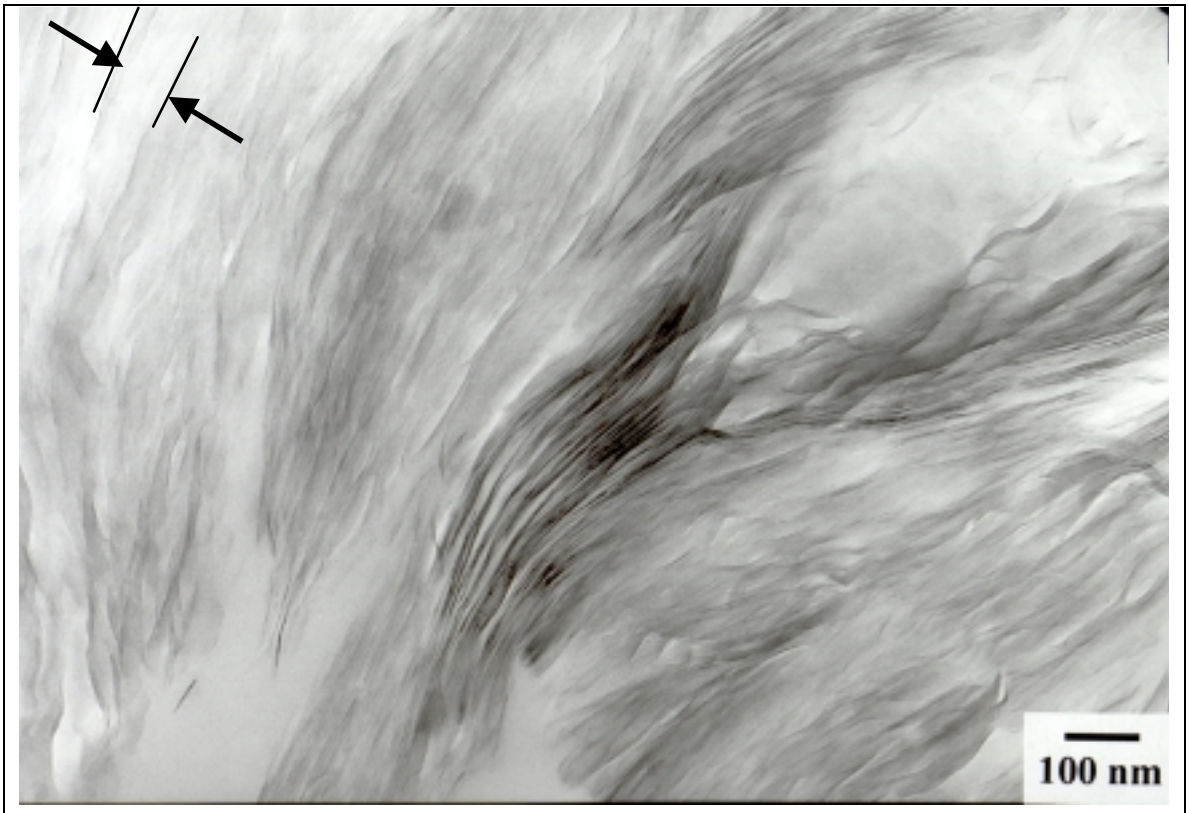

Figure 31 TEM micrograph of exfoliation at 2.5% montmorillonite

It would be reasonable to conclude that the ends of the card-like structures are attracted to each other because they could contain charge polarized regions. The observation of the 45° angle in **Figure 32** appears to support an argument for platelet attraction based on an edge to edge association. Charge non-uniformity may be a mechanism for aggregate formation.

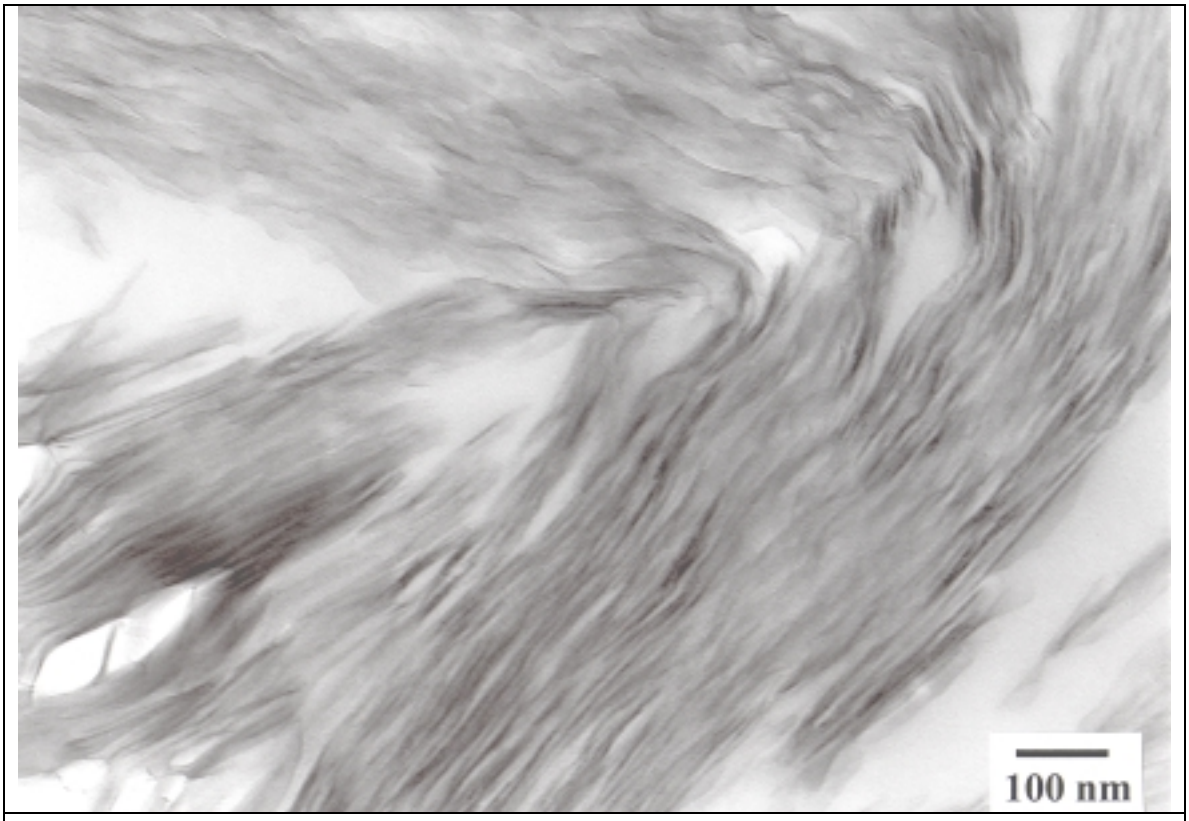

Figure 32 TEM of 45° platelet edge association for 2.5% montmorillonite

The 5% nanoclay was also examined by TEM in **Figure 33** to determine why there might be no large-scale structures. This micrograph indicates a change to a much more compact parallel arrangement of the intercalated regions of nanoclay. Little or no space between these was left for individual exfoliated platelets. This structure is short range, not long range. It is clearly illustrated in this figure that some regions of parallel cards, or intercalated clay plates, have their grains oriented at right angles to others. The appearance of micelles might therefore only be possible when the density of plates do not force the alignment of clay particles into dense structures of parallel and perpendicular sheets. If there is a charge polarization balance at work for this concentration, then the

orientation is not a herringbone end on association, but instead an edge to face type of platelet orientation.

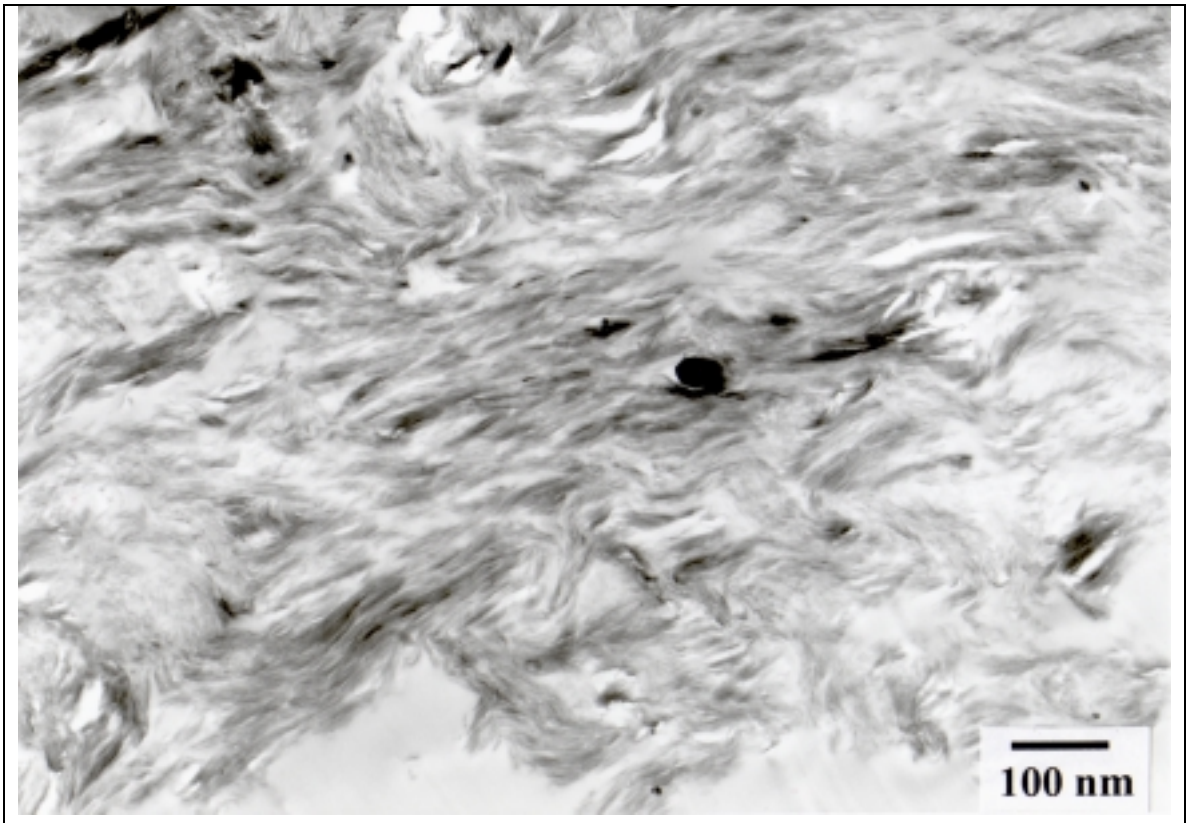

Figure 33 TEM of platelet edge to face association at 5% montmorillonite

CHAPTER 6

PERFORMANCE

6.1 Environmental resistance to moisture

Moisture absorption rate was examined above the T_g based on the relatively large improvement in the shear modulus that was observed above the T_g temperature. Water is a polar molecule, and the nanoclay is a charged system. Any evidence of change in the rates of moisture uptake for different concentrations might indicate the presence of a fundamental change in transport mechanism. The moisture uptake was monitored in accordance with ASTM D5229 as described in the experimental section. The test results in **Figure 34** reflect an average of seven specimens of the same shape, size, and thickness dimension at each concentration. The error that represents one standard deviation of the mean measurement is in each case smaller than the symbol used to mark the data point.

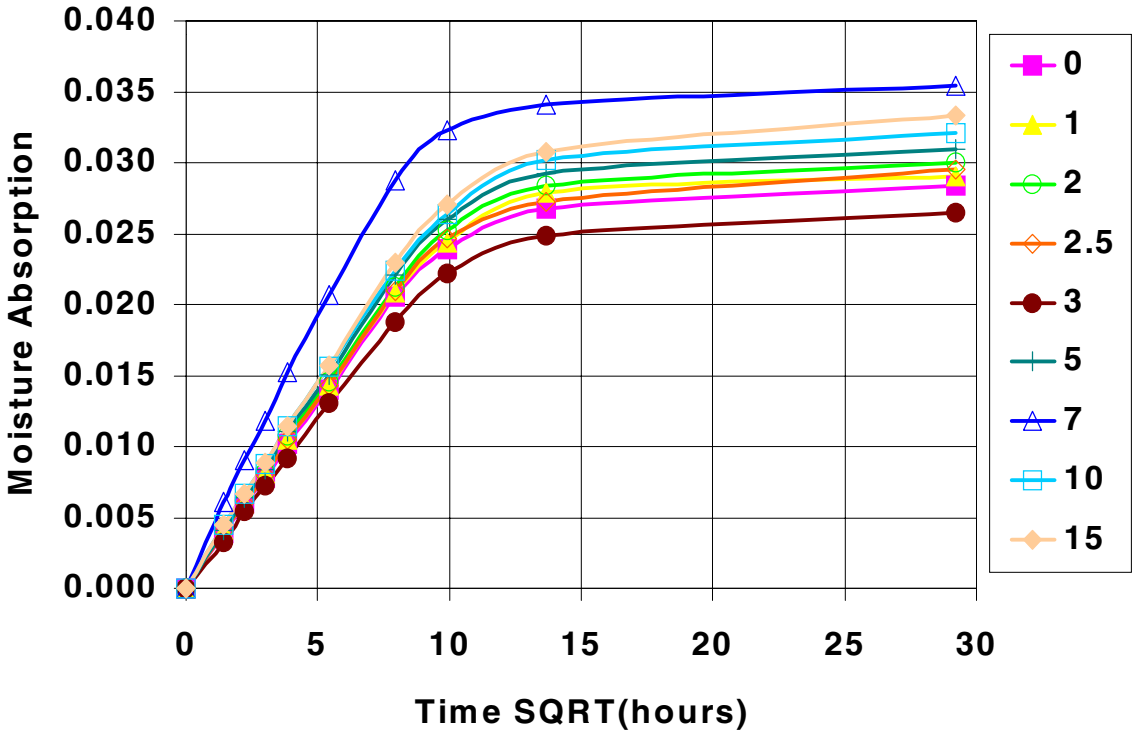

Figure 34 **Moisture uptake plotted according to exposure time.**

The intent of the moisture evaluation was to determine concentration dependent effects. This required that the data from **Figure 34** be plotted as shown in **Figure 35**.

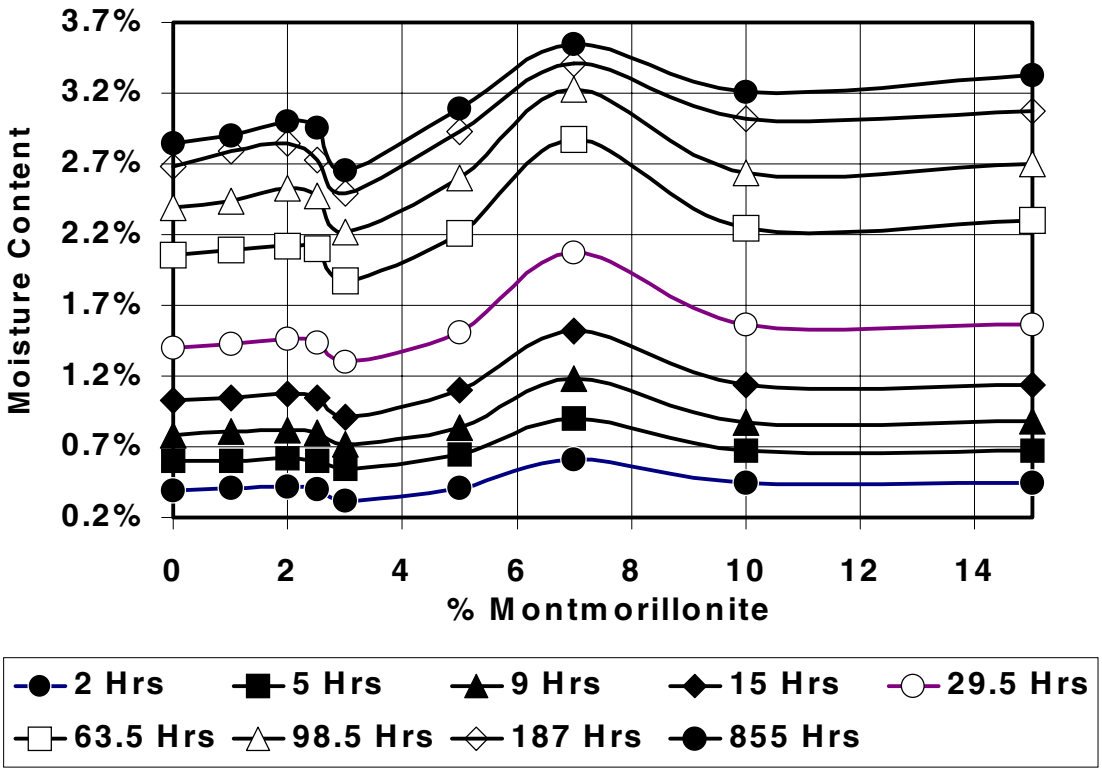

Figure 35 Comparative moisture absorption at 82°C and 95% relative humidity

It is conjectured that the association of individual exfoliated plates in a staggered and brick-like pattern may be responsible to form the water barrier. The unusual result at 3% nanoclay might be attributed to evidence of the barrier effect that was introduced earlier with regard to properties of interest for nanoclay additives. Perhaps at concentrations less than 3% the micelle analogs create large gaps between groups of plates that provide no barrier to water. At 3% concentration the micelles have greatly reduced in size and number. At concentrations above 3% clay the proximity of the dispersed platelets might again enhance conduction of moisture along contacting silicate surfaces to explain the result for concentrations in excess of 3%.

It is also conjectured that the moisture result could be explained in terms of hydrogen bonded surface interaction of water with the clay platelets. Bound water would not diffuse to the extent that unbound water could. Future studies might perform proton nuclear magnetic resonance of nanocomposite as a function of moisture diffusion to clarify the presence and extent of hydrogen bound versus unbound water.

6.2 Tensile Tests of nanocomposite and moisture conditioned nanocomposite

Addition of mica, talc, and other fillers often results in a decrease of the ultimate tensile strength (UTS). It is therefore significant that no change was observed in the ultimate tensile strength of the nanocomposite with clay concentration. Tensile modulus was improved with concentration of nanoclay. It was observed that there was almost no elongation possible prior to tensile failure at and above 5% nanoclay. Mechanical properties are summarized in **Table II** for dry and **Table III** for wet conditioned specimens.

Table II

Mechanical Properties, Room Temperature Dry

no. of test results (n)	%/wt MM	% Elongation at break		UTS (MPa)		Tensile Modulus (MPa)	
		Average	STD DEV	Average	STD DEV	Average	STD DEV
(n=6)	**0**	14.8	2.0	60.0	1.2	1308.1	46.9
(n=6)	**1**	13.3	1.0	61.2	1.5	1374.6	26.5
(n=6)	**2**	13.0	1.4	61.0	0.9	1402.1	21.7
(n=6)	**2.5**	12.4	1.8	61.0	0.4	1427.3	27.2
(n=6)	**3**	9.7	1.5	61.5	1.7	1440.6	42.1
(n=6)	**5**	9.9	0.9	64.1	1.1	1539.3	25.3
(n=6)	**7**	6.9	1.2	61.7	1.9	1565.4	36.5
(n=6)	**10**	6.9	0.4	64.6	0.9	1711.9	44.0
(n=5)	**15**	2.2	0.7	48.2	10.7	2144.5	166.9
Deviation average:			1.2		2.3		48.6

Table III.

Mechanical Properties, Moisture Conditioned

no. of test results (n)	%/wt MM	"WET" % Elongation at break		"Wet" UTS (MPa)		Tensile Modulus "Wet". (MPa)	
		Average	STD DEV	Average	STD DEV	Average	STD DEV
(n=7)	**0**	14.7	1.5	50.9	0.6	1159.6	56.3
(n=6)	**1**	10.9	0.8	51.3	0.7	1232.5	16.1
(n=6)	**2**	9.9	0.9	50.6	1.1	1221.0	36.3
(n=7)	**2.5**	7.0	1.8	48.3	5.0	1223.5	25.8
(n=6)	**3**	7.4	0.6	51.2	0.2	1300.9	22.4
(n=6)	**5**	4.4	1.7	45.8	10.4	1432.9	125.5
(n=7)	**7**	5.4	0.8	44.5	1.4	1278.0	38.1
(n=6)	**10**	4.6	0.4	50.4	1.0	1484.1	37.5
(n=7)	**15**	2.3	0.4	36.7	4.5	1697.4	102.1
Deviation average:			1.0		2.8		51.1

The expected reduction of tensile modulus due to the effect of equilibrium water content, in this case a 13% drop was independent of the concentration of the nanoclay. This result suggests there is no water-clay interaction at the particle-matrix interface that would act to either reduce or improve the ability of the nanoclay to support the matrix.

The tensile modulus at room temperature is best understood by examination of the DMA test results in **Figure 36**.

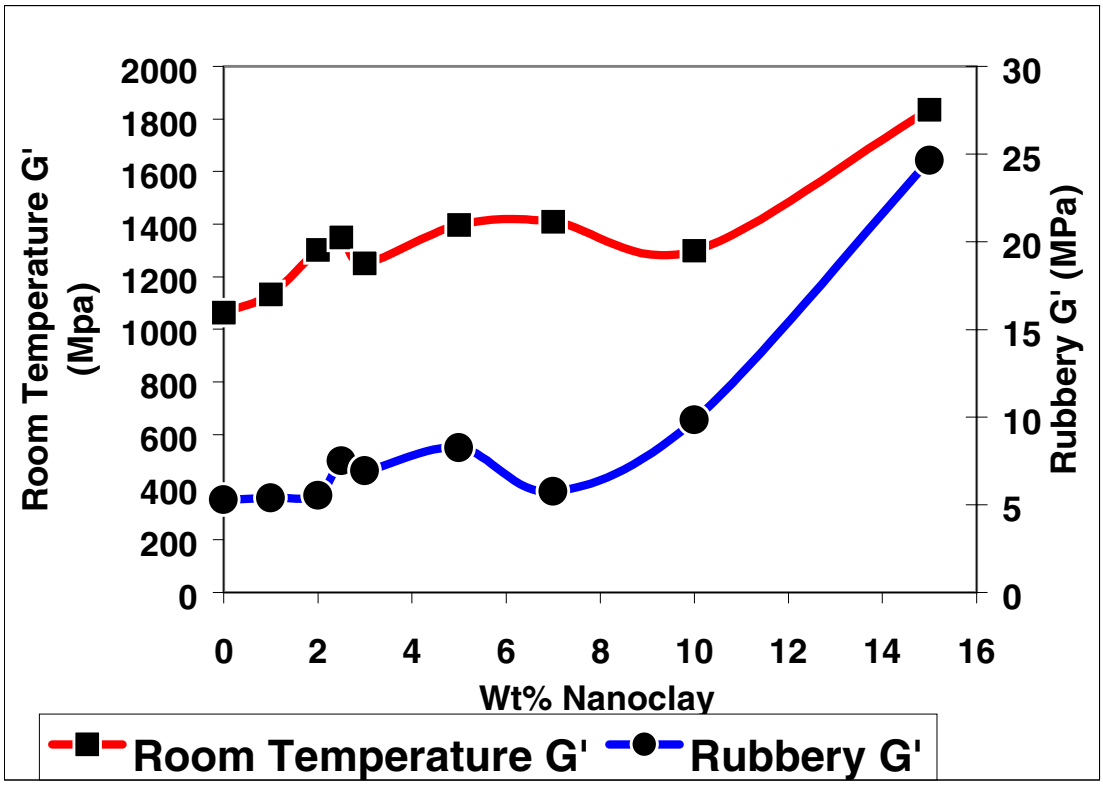

Figure 36 The effect of Nanoclay additive on the improvement of modulus is much greater above T_g and at high concentrations of montmorillonite.

A comparison of the glassy shear modulus at room temperature was made with modulus at the rubbery response region above $T_{g.}$ The best proportion of modulus improvement to that of the unfilled state can be achieved at elevated temperatures and high concentrations of clay.

6.3 DMA of nanocomposite and moisture conditioned nanocomposite

The addition of nanoclay to the epoxy evidenced a strong compositional effect on the T_g by DMA as confirmed by the T_g obtained by DSC. The merit of this comparison is that the DMA measures a mechanical deformation while the DSC measures changes in a thermodynamic quantity. The independent measures help lend credibility to the trend in the result.

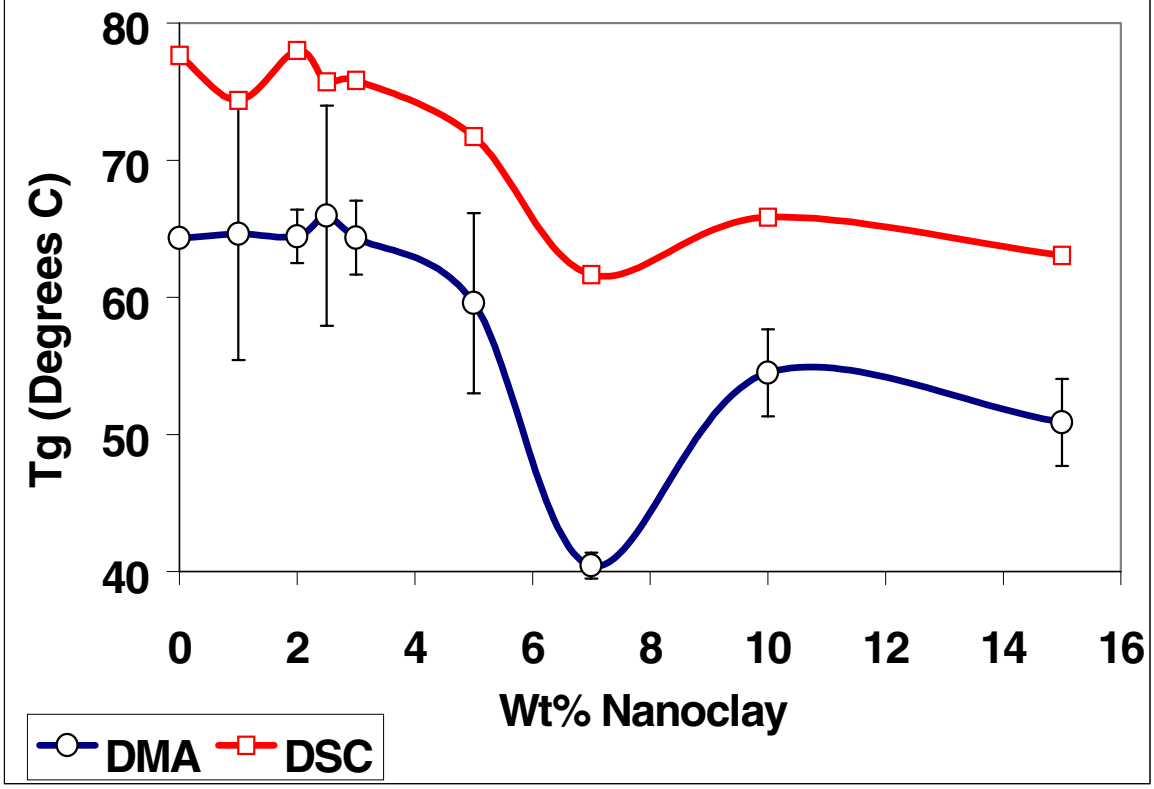

Figure 37 DSC results for T_g compared with DMA results for T_g

As seen in **Figure 37**, the T_g is not influenced by clay concentration below 3 weight percent. Above 3% concentration a strong plasticization of the matrix resin occurs with T_g falling as much as 24°C below that of the base resin for 7% by weight of nanoclay. Above that level, the T_g increases somewhat from the lowest point yet still remains lower than the base resin.

The error bar on the DSC result reflects the goodness of the fit to a transition function that was used to determine the midpoint in the data from a single experiment for each clay concentration.

The storage and loss moduli were plotted against the experimental frequency for each test temperature to generate master curves. The values of the shift factors were then plotted for each temperature. In all cases, there was graphical superposability of both the T_g and the beta relaxation region. Closer examination revealed the T_g region and the beta relaxation region appear to be composed of a single well-resolved relaxation. This system was therefore considered to be thermorheologically simple.

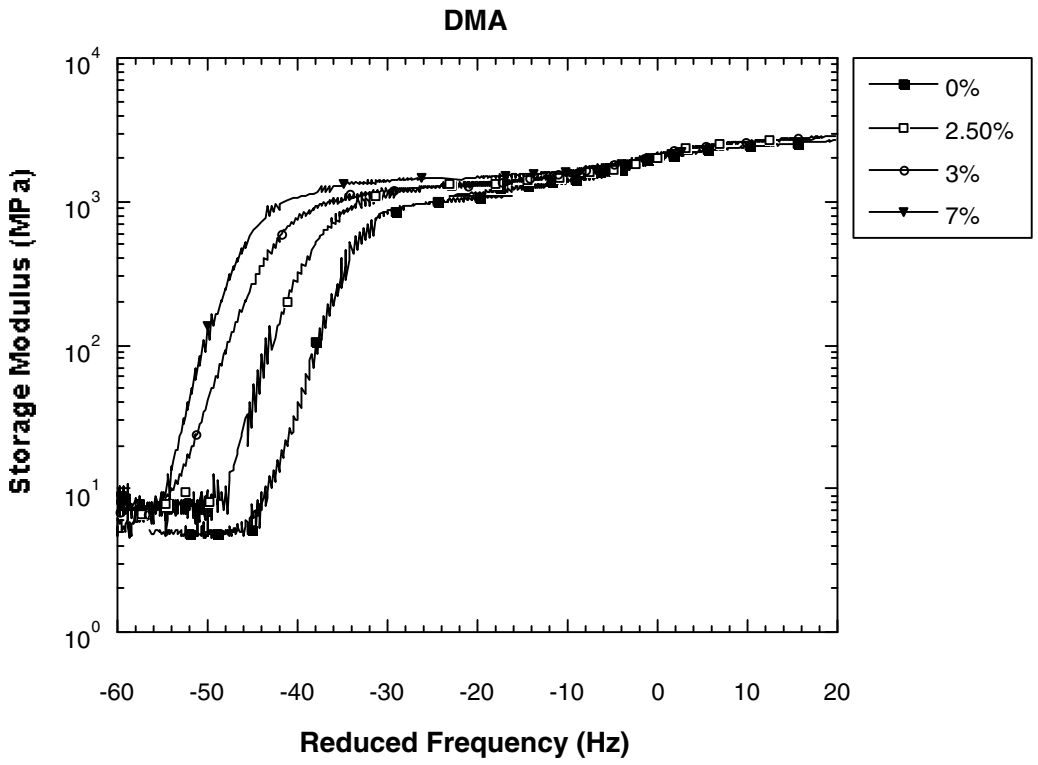

Figure 38 **Elastic modulus master curves for nanocomposites**

A comparison of the elastic modulus master curves is shown in **Figure 38** to observe the effect of composition**.** It can be seen from the figure that the beta relaxation region changes near 0 Hertz are also present but have a lesser response. The alpha transition that is the T_g is at higher temperature than the beta relaxation region, so it appears here at a lower reduced frequency. The T_g concept was introduced as the polymer backbone rotation that accounts for the largest change in a polymer material of from stiff to rubbery response. The trend to a more rubbery material indicates the addition of clay has a plasticizing effect on the composite, which is detrimental to the

performance of the matrix when elevation or at least maintenance of T_g is a critical criteon.

The beta relaxation was described as the transition region associated with group rotation pendant from the polymer molecule. The significance of a change in the beta transition is that it has been used in the past (42) to correlate quantitatively with polymer room temperature impact resistance along with other evidence such as a distinct storge modulus drop in the range of the beta transition as was seen in **Figure 38.**

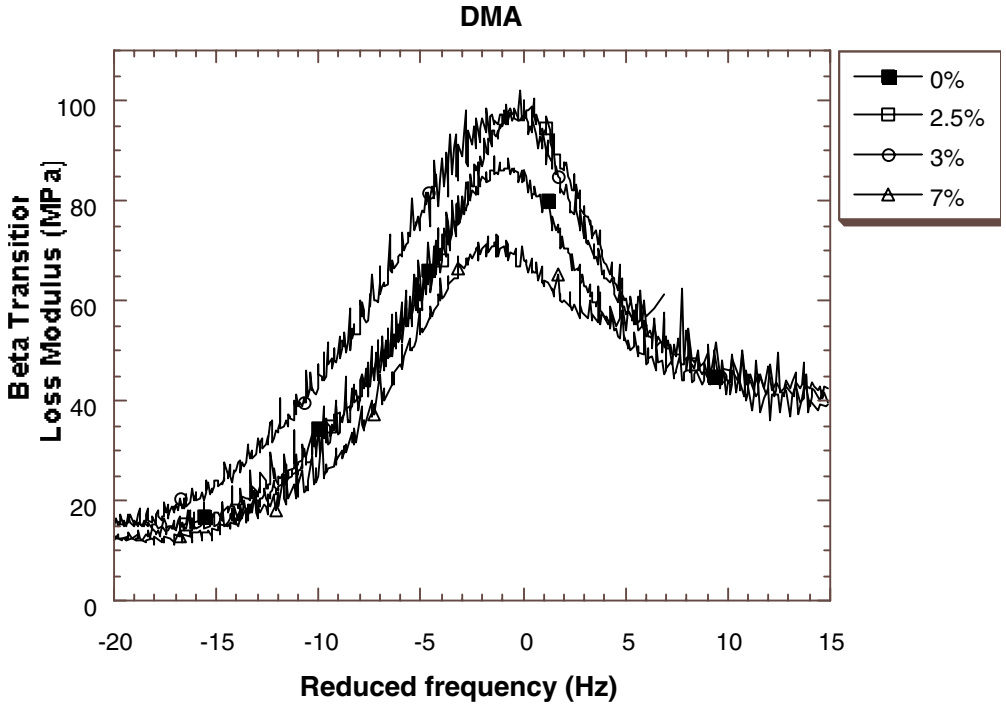

Figure 39 Beta transition loss modulus response for nanocomposites

As can be seen from the expanded view of the loss modulus master curves corresponding to the beta relaxation region in , a shift in the modulus to lower reduced frequency was evident with increase in nanoclay concentration. This indicates that some

restriction in the beta relaxation region occurs upon nanoclay addition. The intensity of the loss modulus in this region also increases. This indicates a higher energy absorbing mechanism as the nanoclay is added. The likely cause of this is friction between the polymer and the reinforcement.

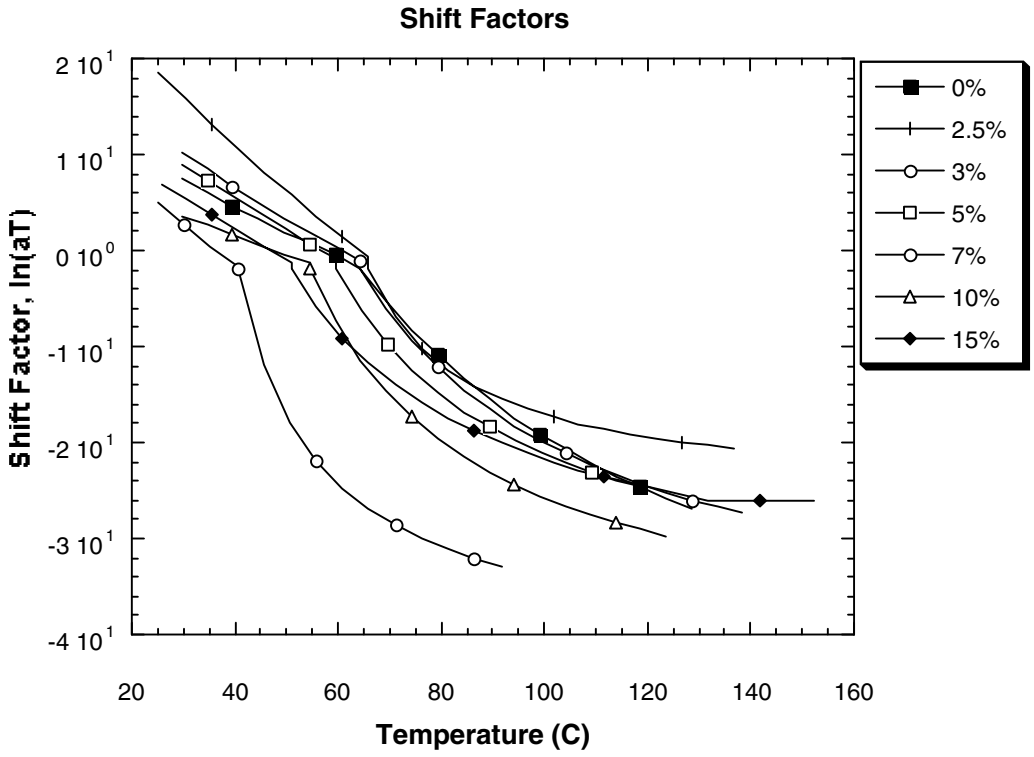

Figure 40 Fitted shift factors depend on clay concentration near the T_g

Around the region of T_g there is a concentration dependence on the shift factors as can be seen in

. A steeper slope of the shift factor versus temperature curve below T_g indicates a concentration dependence of flow activation. The knee of the two fitted shift factor regions indicates the reference temperature for shift. The reference frequency used for

this analysis was 0.159 Hertz (1 radian/second). The flow activation energy - composition analysis for temperatures just below the T_g are shown

in **Figure 41**

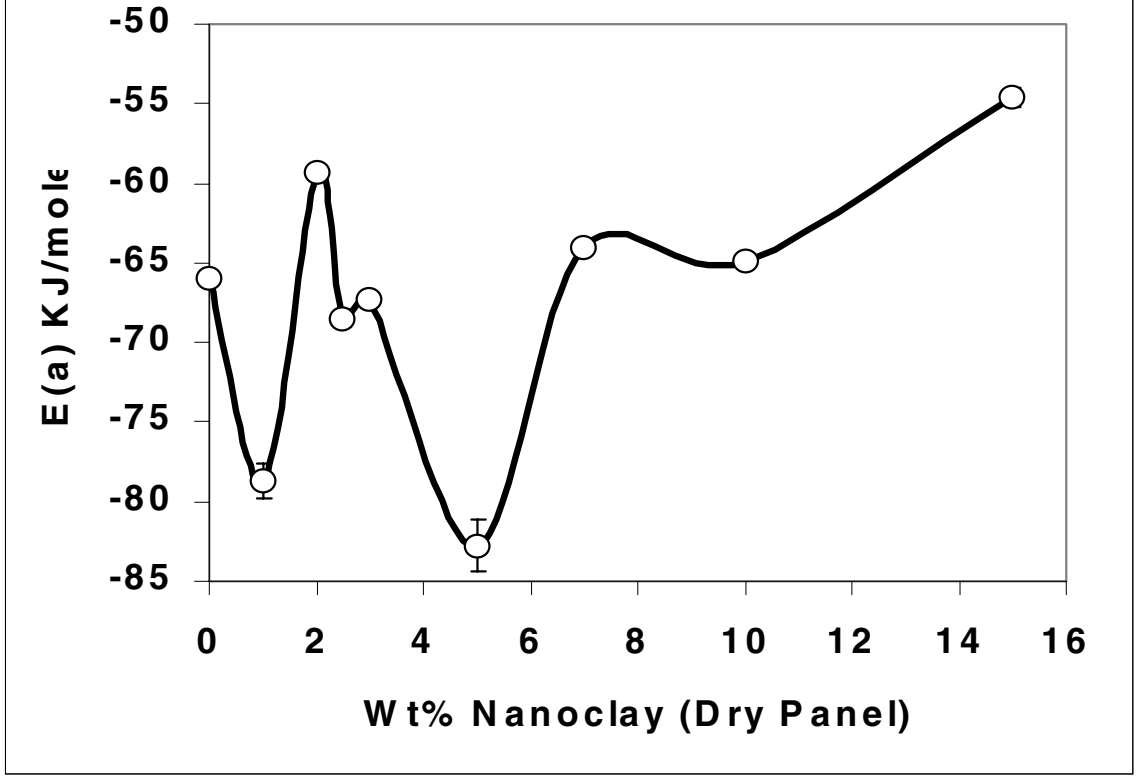

Figure 41 Flow Activation E(a) for beta relaxation region observed for dry conditioned nanocomposite as a function of montmorillonite concentration.

As can be seen for compositions above 3% nanoclay there is an increase in the activation energy barrier for segmental flow of the epoxy. This is interesting given the low T_g value at 7% nanoclay. This indicates that the increase in flow activation energy is not driven by intrinsic effects due to the matrix but rather due to packing and distribution of the individual silicate platelets in the epoxy. In future work, elevated temperature tensile tests conducted above the T_g would be expected to lend credibility to this result.

To understand the post T_g results on flow behavior, the Williams-Landel-Ferry equation (W-L-F) is utilized. Narrow confined spaces between silicate platelets may be sufficient to constrain the motion of polymer entrapped between them, the changes in C_1 and C_2 for the T_g as a function of nanoclay concentration were examined in **Figure 42**.

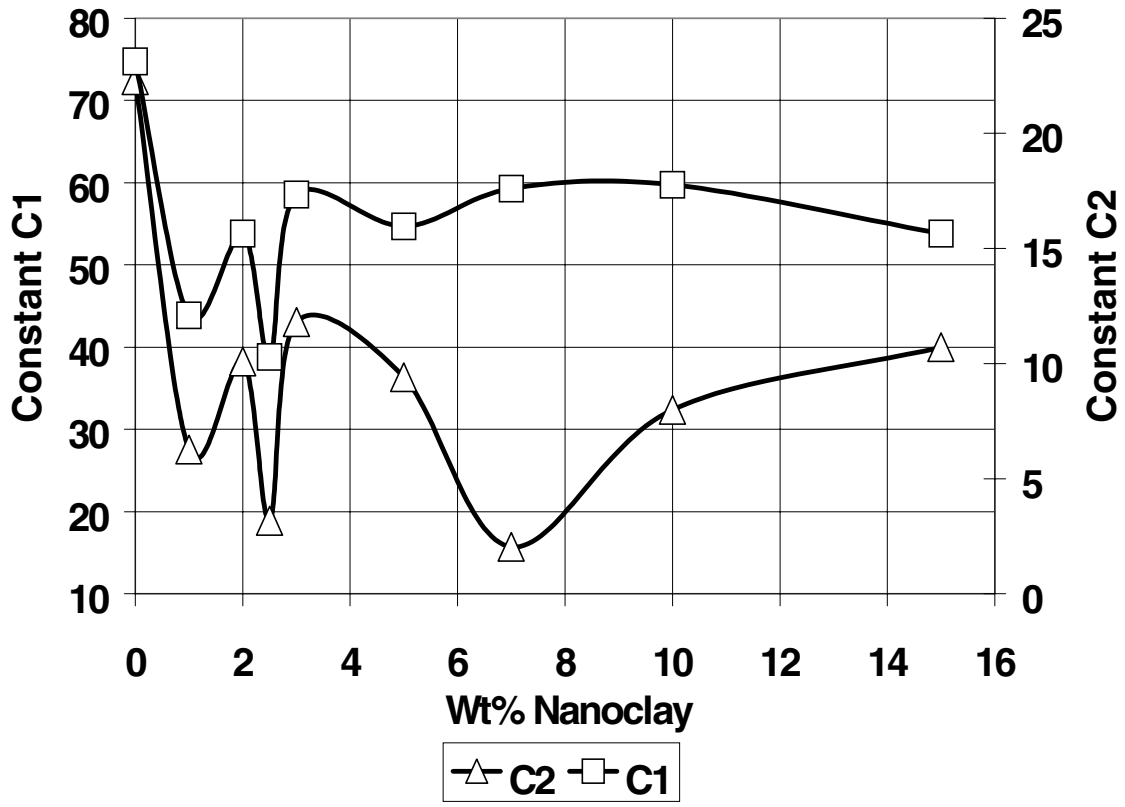

Figure 42 WLF constants change as a function of montmorillonite Concentration above T_g.

As can be seen for all compositions the values are lower than the base resin. The overall results indicate that the effect of nanoclay presence is most dramatic in the post T_g

region. The reduced values of the WLF constants at 2.5% and 5% by weight indicate these clay compositions have the largest ability to reduce polymer free volume.

The shape of the dispersed particle geometry generally dictates the type of reinforcement mechanism expected in composite systems. A key issue in micromechanics has been to try to link macroscopic behavior to microscopic field variables. This subject has been treated exhaustively in a textbook collection of works edited by Oda and Iwashita (43). The flat platelet geometry in clay nanocomposites would expect its best reinforcement at large strains. Large strain would change the contact angle on the flat dispersed particles to point their normal directions closer to the direction of the major principle stress. The modulus observed here for the tensile test supports this result. The magnitude of change in the shear modulus for any given constant frequency of test was not significant by DMA because of the small strain (0.1%) used to test these samples. Use of multiple frequencies at small strain, however, was able to detect differences in response due to the particles.

Interaction between polymer molecules and the surfaces of non-symmetric particle reinforcement would be expected to become more prominent above the glass transition temperature. This is where frictional polymer motion across the surface is possible and rolling particle orientation is also possible. Below the T_g the polymer motion is reduced as the polymer begins to take the load of deformation.

The beta relaxation was selected for this analysis rather than the T_g because this region was not subject to the loss of water on test over the temperature range of interest for the studied system. Water can act as a lubricant at the interface between the nanoclay

and the non-bonded portions of matrix polymer to remove a large component of friction. Water also can act to swell the resin, fill voids, and thus bind particles from free rotation.

The beta relaxation region flow activation energy was reduced 19 KJ/mole in the wet conditioned panels from that determined for the dry panels. DMA tests of wet and dry elongationally oriented samples at different strains help sort out the contribution of polymer sliding friction from that of molecular rotation and molecular re-orientation and configuration as shown in **Table IV.**

Table IV

Wet Vs. Dry Flow Activation for the Beta Relaxation

% Weight Nanoclay		2.50%	2.50%	2.50%		0%	0%	0%
	Strain	Flow Ea KJ/mol	Goodness of fit	(+/-) E(a)		Flow Ea KJ/mol	Goodness of fit	(+/-) E(a)
Dry	0.1%	-69.7	0.9913	0.6		-67.4	0.9971	0.2
Dry	0.5%	-52.0	0.9981	0.1		-48.5	0.9934	0.3
Dry 1.06% pre-elongated	0.1%	-47.1	0.9990	0.0		-56.1	0.9959	0.2
Dry 1.06% pre-elongated	0.5%	-47.2	0.9920	0.4		-43.9	0.9922	0.3
Wet	0.1%	-55.5	0.9991	0.0		-54.3	0.9983	0.1
Wet	0.5%	-46.0	0.9904	0.4		-50.4	0.9967	0.2

Here, wet and dry panels have no statistical preference for the error analysis in either case. The E_a response is 35 times larger for all wet conditioned specimens, however. This lends credibility to the use of the set of wet panels E_a to make a relative comparison of the concentration dependence on the activation of flow, which is a significant result because it increases understanding of how to evaluate these systems.

For these reasons the traditional determination of E_a used to compare the effect of concentration dependence previously shown in **Figure 41** invites comparison with the wet conditioned E_a shown in **Figure 43**.

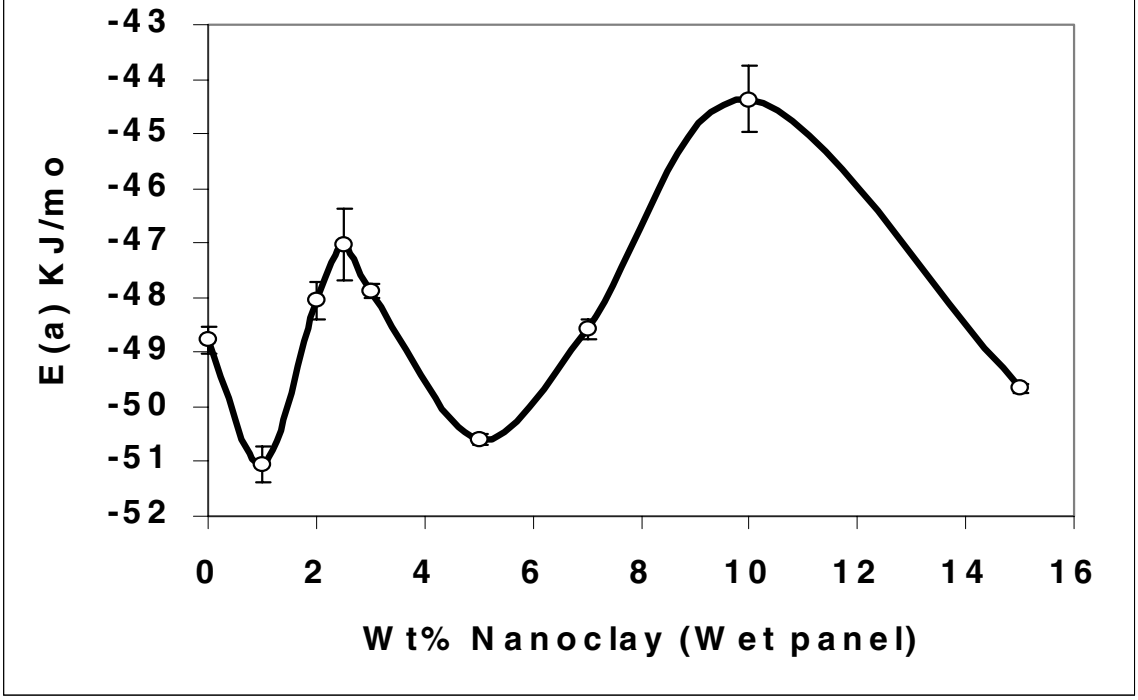

Figure 43 Flow Activation E(a) for beta transition observed for wet conditioned nanocomposite as a function of nanoclay concentration

CHAPTER 10

SUMMARY

10.1 Effect of montmorillonite concentration on epoxy kinetics

Determination of the chemical activation energy showed that the presence of the treated clay did not significantly alter the overall energy of the reaction. This indicates a conservation of stoichiometery. The frequency factor indicated no diffusion or surface environment mediation of the reaction based on differing heating rates observed for each clay concentration. This demonstrates equivalence of inter-gallery and extra-gallery chemical reactions. Depression of the temperature of the maximum rate of the reaction of epoxy and amine hardener was significant for all clay concentrations tested with the recurrent exception of 2.5% clay. This anomaly was observed at all heating rates tested.

SEM results indicate the maximum size and greatest occurrence of the unexpected spherical agglomerates resembling micelles was at 2.5% clay in the nanocomposite. The greatest tendency to form a layered morphology appeared at 10% clay. Slow stirring as well as ultrasonic treatment of the premix was uniform for each preparation, yet the spherical agglomeration of clay platelets varied in size and distribution across concentrations. When the correspondence of the chemical kinetic rate at 2.5% is considered together with the maximum particle agglomeration at 2.5%, it must be concluded that the particle charge distribution was primarily influenced by the rate of growth of the epoxy polymer chains.

10.2 Concentration effects on distribution and exfoliation

The absence of peaks in the x-ray spectrographs corresponding to the interlayer d-spacing of the montmorillonite showed that for all concentrations the intergallery order was disturbed. However for montmorillonite concentrations above 2.5%, leading edge analysis of the spectra indicated that the spacing had increased beyond that of the pure of montmorillonite but beyond the detectability of the wide angle x-ray diffraction instrument used. This conclusion was validated through the TEM micrographs where interlayer spacing of 60 to 30 nm was observed with increasing montmorillonite concentrations.

TEM results indicate a loosely packed herringbone pattern of the partly intercalated platelets that are oriented end to end at 2.5% concentration, and a tightly packed right angle pattern in platelets that are oriented edge to face at 5% concentration. Even though the clay was both exfoliated and partially intercalated at both concentrations, X-ray results correlated well with the micrographs indicating limits to the degree of exfoliation above 2.5% montmorillonite. This correspondence of the change in the microstructure and in the bulk exfoliation explains the very different clay structures observed at long range by SEM.

10.3 Effect of montmorillonite on mechanical properties

Significant reinforcement was indicated by an improvement to modulus as well as a retention of ultimate tensile strength for increasing clay concentrations. The agglomerated particles seen by SEM in the greatest quantity at 2.5% clay concentration were insufficient to dominate the matrix failure, as were the platey structures seen at other concentrations. This was confirmed when moisture saturated samples showed

lower moduli due to the epoxy matrix independent of clay concentration. The reason for this is attributed to the evidence provided by TEM that exfoliation was not complete.

A depression of the nanocomposite T_g was observed by DMA for concentrations greater than 5% clay. This was accompanied by reduced elongation to failure measured by tensile testing. The latter effect results from a decrease in the amount of the exfoliated state for greater than 5% concentrations of clay. The trend to a more rubbery material indicates the addition of clay has a plasticizing effect on the composite. The DMA results indicate improvement in the rubbery modulus, an increase in the energy absorption in the beta transition region, and an increase in the activation energy of flow that are positive improvements to performance.

The reduction in the relaxation time determined by DMA at 7% clay is due to the layered structure. An increase in flow activation energy at this composition where T_g is reduced indicates this effect is not due to the matrix, but is due to the filler dispersion. The DMA damping absorbance follows the increase of clay concentration with an increase in damping magnitude at the Tg. The path independence of the DMA modulus measurements indicated no breakdown or alteration of physical or chemical microstructure resulted on application of a thermal history or a mechanical deformation at any concentration of clay. As clay concentration is increased, both the drop in the WLF constants above T_g as well as the change in the DMA rubbery modulus indicate that nanoclay reinforcement will be most effective at temperatures greater than the T_g region.

10.4 Effect of moisture on nanocomposites

The decrease in tensile properties due to moisture was independent of clay concentration. The resin matrix rather than the clay reinforcement dominated the nanocomposite mechanical properties as inferred from the similarities in trends between the rising tensile modulus in dry and moisture conditioned samples. The consistently improved properties at 2.5% nanoclay imply improved impact resistance of exfoliated silicate nanoclay composites may exist over an unexpectedly narrow range of concentration.

APPENDIX I

RECCOMENDATIONS FOR FUTURE RESEARCH

Better exfoliation of montmorillonite in epoxy

An investigation of secondary amine alkylammonium cation reaction with epoxy monomer in montmorillonite silicates needs to be made to see if a crosslink reaction rather than a homopolymerization of the monomer is possible. It has already been found that secondary amine alkylammonium cations intercalate as well as primary amine alkylammonium cations (8). The reduced exfoliation reported in the initial comparative investigation (8) may have been caused by a failure to properly account for an altered stoichiometry due to the competitive reaction of secondary amine alkylammonium cations in covalent combination with epoxy. Proper stoichiometry by a reduction of the amount of hardener added may therefore significantly increase the amount exfoliation possible in epoxy. Some evidence for this possibility was suggested by an analogous reaction of epoxy with silicic acid treated with tertiary amine alkylammonium cations.

Population and distribution of particle aggregates at 2.5% clay concentration

The effect of slow stirring without ultrasound and the effect of supplementary ultrasonic treatment of the premix should be compared. This would establish the importance of shear forces or steric considerations on the rate of aggregate particle formation.

Measure of platelet orientation

Anisotropically improved properties might be expected if the particulates were preferentially oriented. The x-ray diffraction response of nanoclay systems under different amounts of elongational stress is therefore of interest to determine if the x-ray diffraction peaks might reappear under some conditions due to local structural change.

Mechanism of moisture transport

Perform proton nuclear magnetic resonance at 3% nanoclay as a function of moisture diffusion time to confirm or deny if a bound versus unbound water diffusion mechanism may exist near the surface charge of the clay platelets. Once the mechanism is better understood, then those concepts may be used to design that property into other concentrations and other nanocomposites.

REFERENCE LIST

1. L. M. Sherman, *Plastics Techn*., **45**, No.6, 52 (1999)

2. Z. Wang, T.J. Pinnavaia, *Chem. Mater.,* **10**, 1820 (1998)

3 R. A. Vaia, B. B. Sauer, O. K. Tse , E. P. Giannelis, *J. Polym. Sci. Polym. Phys.* **35**, 59 (1997).

4 H. van Olphen, *An Introduction to Clay Colloid Chemistry*, John Wiley and Sons, New York (1963)

5 R. Krishnamoorti, E. P. Giannelis, *Macromolecules*, **30**, 4097 (1997).

6 E. P. Giannelis, Adv. Mater. **8**, No. 1, (1996)

7 M. S. Wang and T. J. Pinnavaia, *Chem. Mater*. **6**, 468 (1994)

8 T. Lan, P. D. Kaviratna, T.J. Pinnavaia, *Chem. Mater.* **7**, 2144 (1995)

9 T. J. Pinnavaia, *Science*, **220**, no. 4595, 365, (1983)

10 T. Lan, Y. Liang, G. W. Beall , K. Kamena, *Additives'99*, San Francisco, CA (1999)

11 S. D. Burnside, E. P. Giannelis, *Chem. Mater.*, **7**, No. 9, 1597 (1995)

12 T. J. Pinnavaia, *Science* **220**, No. 4595, 365 (1983)

13 Z. Wang, T. J. Pinnavaia, *Chem Mater*. **10**, 3769 (1998)

14 R. A. Vaia, K. D. Jandt, E. J. Kramer, E. P. Giannelis, *Macromolecules* **28**, 8080 (1995)

15 R. A. Vaia, E. P. Giannelis, *Macromolecules* **30**, 7990 (1997)

16 E. P. Giannelis, R. Krishnamoorti, E. Manias, *Adv. Polym. Sci*, **138**, 108 (1999)

17 P. B. Messersmith, E. P. Giannelis, *Chem. Mater.* **6**, 1719 (1994)

18 T. Lan, T. J. Pinnavaia, *Chem. Mater*. **6**, 2216 (1994)

19 T. Lan, P. D. Kaviratna, T. J. Pinnavaia, *J. Phys. Chem. Solids* **57**, 1005 (1996)

20 Z. Wang, T. J. Pinnavaia, *Chem. Mater*. **10**, 1820 (1998)

21 N. A. Prakash, Y. M. Liu, and B. Z. Jang, *Polym. Comp.*, **15**, No. 6, 479 (1994).

22 B. Geisler, F. N. Kelly, *J. Appl. Polym. Sci.* **54**, 177 (1994)

23 D. Shia, C. Y. Hui, S. Burnside, and E. P. Giannelis, *Polym. Comp.* **19**, No.5, 608 (1998)

24 X. Kornmann, L. A. Berglund, J. Sterte, and E. P. Giannelis, *Polym. Eng. Sci.*, **38**, No. 8, 1351 (1998)

25 T. Lan, G. Beall, K. Kamena, Additives '99, San Fransisco, CA. March 22-24, (1999), submitted for publication.

26 R. W. Rice, *J. Matl. Sci.*, **32**, 4731 (1977)

27 C. L. Soles, F. T. Chang, D. W. Gidley, A. F. Yee *J. Polym. Sci. B*, **38**, 776 (2000)

28 C. L. Soles, A. F. Yee, *J. Polym. Sci. B*, **38**, 792 (2000)

29 K. Iko, Y. Nakamura, M. Yamaguchi, and N. Imamura, *IEEE Elec. Ins. Mag.*, **6**, No. 4, 25, (1990).

30 M. C. Leh, N. A. Peppas, *J. Comp. Matls.*, **27**, No. 12, 1146 (1993)

31 T.S. Chow, *J. Phys. Condens. Matter,* **10** L445 (1998)

32 Harrowell, eds. S. Manne, and G.Warr, *Supramolecular Structure in Confined Geometries*, Am. Chem. Soc. Washington, D.C. (1999), Symp. Series 736, Chapt. 7.

33 See Ref. 32, Chapt. 1

34 Nanocor Dispersion Guideline T-13 for Nanomer I.30.E

35 H. Eyring, Rheology: Theory and Applications, (eds. F.R Eirich), Academic Press, New York (1956), Pp 273-274, 327, 334, 469-470

36 J.D. Ferry, Viscoelastic Properties of Polymers, 3rd Ed., John Wiley & Sons, New York (1980), Pp 285-289.

37 P. B. Messersmith, E. P. Giannelis, *Chem. Mater.* **6**, 1719 (1994)

38 Edwin P. Plueffemann, Silane Coupling Agents, Plenum Press, New York, (1982), Pp 17-20, 135, 167, 207.

39 *ASTM E698* Arrhenius Kinetic Constants for Thermally Unstable Materials.

40 Edith Turi, *Thermal Characterization of Polymeric Materials, 2 Ed.*, Academic Press, N.Y. (1981) Pp. 1642

41 P. Somasundraran, B. Markovic, S. Krishnakumar, and X. Yu, eds. K.S. Birdie, Handbook of Surface and Colloid Chemistry, CRC Press, Boca Raton, Florida (1977), Chapt. 14, Pp 559-601.

42 G. Menges, H. Boden, eds. W. Brostow, R.D. Corneliussen, *Failure of Plastics*, Hanser Publishers, N.Y., (1986), Pp 179-183.

43 M. Oda, K. Iwashita, eds., *Mechanics of Granular Materials, an Introduction*, A. A. Balkema Publishing, Rotterdam, Netherlands (1999), Pp 177, 226-232, 306-308.